Photosynthetically Active Radiation Separation Model for High-Latitude Regions in Agrivoltaic Systems Modelling

S. Ma Lu [1, *], D. Yang [2], M. C. Anderson [3], S. Zainali [1], B. Stridh [1], A. Avelin [1], P. E. Campana [1, *]

1 Mälardalen University, Department of Sustainable Energy Systems, Västerås, Sweden

2 School of Electrical Engineering and Automation, Harbin Institute of Technology, Harbin, Heilongjiang, China

3 USDA ARS, Hydrology and Remote Sensing Laboratory, Beltsville, MD, USA

Corresponding author: silvia.ma.lu@mdu.se

Abstract

Photosynthetically active radiation is a key parameter for modelling the photosynthetic behaviour of plants in response to sunlight and, subsequently, for determining crop yield. Separating photosynthetically active radiation into direct and diffuse components is of significance to agrivoltaic systems, which combine solar energy conversion and agricultural farming on the same portion of land. Placing photovoltaic on agricultural land results in varying shading conditions throughout the day and seasons, producing a higher contribution of incident diffuse radiation to the crops beneath the system in these shaded regions. Additionally, photosynthesis is more efficient under conditions of diffuse radiation than direct radiation per unit of total photosynthetically active radiation. This study introduces a new separation model capable of accurately estimating the diffuse component from the global photosynthetically active radiation and conveniently retrievable meteorological parameters. The model builds upon one of the currently most performing separation models for decomposing global solar radiation into diffuse radiation, the YANG2 model. Four new predictors, found relevant in the literature to influence diffuse photosynthetically active radiation, are added: optical thickness, vapour pressure deficit, aerosol optical depth, and surface albedo. The proposed model has been calibrated, tested, and validated at three sites in Sweden with latitudes above 58° N, outperforming four other models in all examined locations, with R^2 values greater than 0.90. To alleviate the scarcity of photosynthetically active radiation studies in high-latitude regions, the seasonal trends and variation of the various radiation components are analysed. To demonstrate the applicability of the developed model, the location of Sweden's first agrivoltaic system is used to assess a variety of cases that take into account the various data availability that is representative of current and future agrivoltaic systems. In cases where in-situ measurements of diffuse photosynthetically active radiation are not available, the results indicate that the model can be utilised and adjusted for adjacent stations. Utilising predictor values derived from satellite data is an alternative method, but the spatial resolution must be considered with caution.

Keywords: photosynthetically active radiation, separation models, direct and diffuse, ICOS, CERES, agrivoltaics

1. Introduction

In land-based ecosystems, carbon uptake is primarily influenced by solar radiation during the daytime (Li et al., 2020). Photosynthetically active radiation (PAR) is the solar irradiance in the spectral interval between 400 and 700 nm (McCree, 1972, 1971). PAR plays an essential role in plant photosynthesis and associated processes, such as greenhouse gas generation by crops or biomass production (Keane et al., 2018; Tan et al., 2018). The knowledge of PAR helps one to estimate the plant's primary production (Mercado et al., 2009). Like the global horizontal irradiance (GHI), PAR can also be partitioned into its diffuse ($PAR_{diffuse}$) and direct (PAR_{direct}) components. This separation is of particular interest to many applications, especially for PAR estimation over land with complex topography, where the surrounding features can block the direct PAR component in an intricate and time-varying way (Olseth, 1997; Wang et al., 2006). Another application of this diffuse–direct separation of PAR is to study PAR distribution in plant canopies, where the diffuse light penetrates to a greater depth within the canopies than does the direct light (Mariscal et al., 2004). Furthermore, the light-use efficiency of plant canopies increases under cloudy conditions, due to the enhancement of the PAR diffuse component (Gu et al., 2002; Kanniah et al., 2012; Mercado et al., 2009). Li et al. (2020) studied the influence of diffuse PAR radiation in a desert steppe ecosystem and concluded that the maximum canopy photosynthesis was reached under cloudy skies.

The implication of PAR separation becomes more profound in the field of agrivoltaic (AV) systems. The agrivoltaic system is a novel concept that combines solar photovoltaic and agricultural activities on the same land area. Agrivoltaic technology is an efficient, effective, and innovative solution to tackling land use competition (Adeh et al., 2019). Nonetheless, one important concern of using such systems is that, for the coexistence of solar energy and agricultural farming, crop yield must not go below tolerable limits. It is known that shading generally decreases crop yield, and different crops behave differently under shading conditions (Barron-Gafford et al., 2019). In open-field AV systems, the amount of PAR reaching the agricultural land is not homogeneously distributed. The solar modules installed in the system produce variable levels of shading directly on the crops throughout a day and over a year. In these shaded areas, the diffuse component of PAR plays a dominant role (Figure 1). Therefore, knowing the amount of diffuse and direct PAR incident to a specific crop area beneath the AV system implies a more accurate crop yield estimation. Noticeably, the studies by Willock et al. (2020), Campana et al. (2021) and Williams et al. (2023) are among the first works in AV systems that introduced the concept of PAR separation for calculating ground light distribution and crop yield; the topic of concern is an exceedingly recent one. Other

agrivoltaic systems modelling studies have employed separation models of GHI, such as Orgill and Hollands (1977) and Skartveit and Olseth (1987), to extract the ground light collection and used the full-spectrum global and diffuse solar radiation as input to crop models rather than global and diffuse PAR (Sojib Ahmed et al., 2022; Valle et al., 2017).

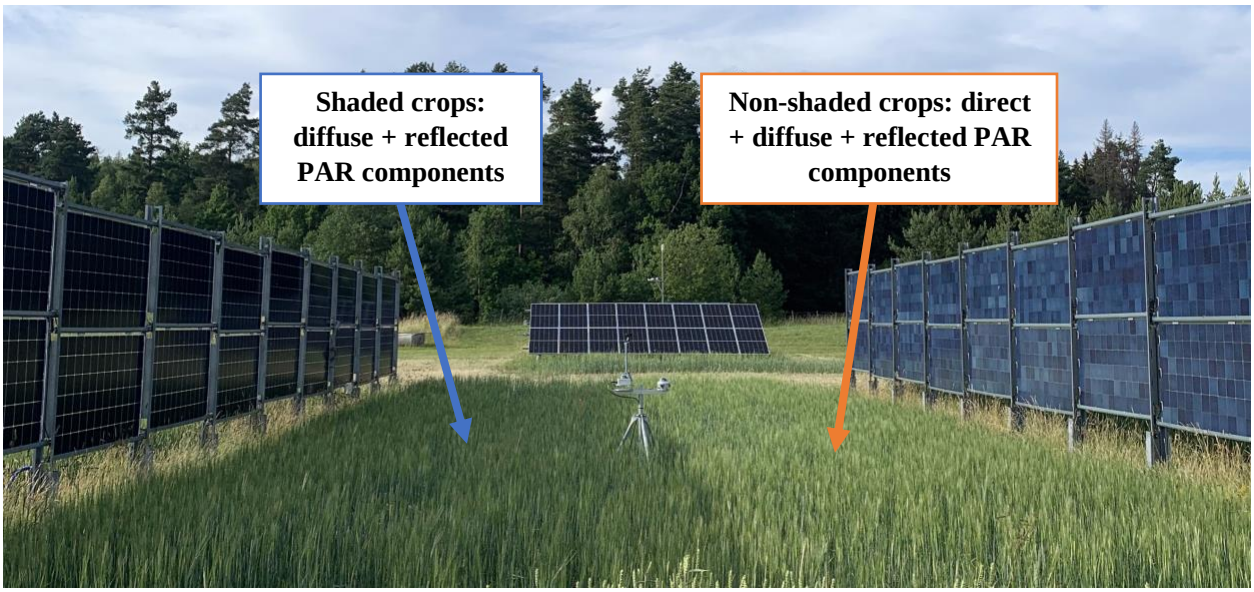

Figure 1. Schematic of photosynthetically active radiation components received at crop level in shaded and non-shaded conditions in a vertical bifacial AV system located in Sweden.

Despite the relevance of PAR on crop growth, the scarcity of PAR measurements and the lack of a worldwide measurement network with standardised quality control protocols (Ferrera-Cobos et al., 2020; Mizoguchi et al., 2010; Niu et al., 2019; Wang et al., 2016) directly explain the limited number of studies about PAR thus far as compared to, for example, the more extensive studies of GHI or diffuse horizontal irradiance (DHI) (Oliveira et al., 2002; Soares et al., 2004; Wong and Chow, 2001). The lack of measurements is even more pronounced for the diffuse component of PAR. Therefore, as a work-around, several authors have suggested a variety of models to estimate the different components of PAR. PAR components can be estimated using atmospheric radiative transfer models (ARTM), e.g., Bird and Riordan (1986), Gueymard (1995) or Emde et al. (2016) and methods derived from these, e.g., Wandji et al. (2019) or Thomas et al. (2019). However, since ARTMs can be highly complex and require extensive knowledge in the atmospheric sciences, most of the models used for applications in the field are empirical. These empirical models can derive the global component of PAR, and a limited number can also derive diffuse PAR (e.g., Weiss and Norman, 1985, Kathilankal et al., 2014), from parameters commonly measured at weather stations (e.g., Alados et al., 1996, López et al., 2001, Hu et al., 2007,), from spectral band measurement (e.g., Trisolino et al., 2016), and from satellite data (e.g., Su et al., 2007, Janjai et al., 2011, Hao et al., 2019). The exhaustive review by Nwokolo et al. (2018) offers an overview of empirical models

to estimate the global PAR (i.e., $\mathrm{PAR_{global}} = \mathrm{PAR_{diffuse}} + \mathrm{PAR_{direct}}$). It is worth mentioning that the correlation between PAR and meteorological parameters is location-dependent (García-Rodríguez et al., 2020).

Several works have focused on the ratio global PAR/GHI and its behaviour in different climate zones. According to the review by Noriega et al. (2020), the ratio is typically higher during summer and lower during winter, though exceptions to this rule have been highlighted by Yu and Guo (2016) or and Ma Lu et al. (2022). Analysis of the global PAR/GHI ratio under cloudless conditions shows a clear dependence on air mass (González and Calbó, 2002). However, under all-sky conditions, the dependence of the ratio is unclear. Yu et al. (2015), Akitsu et al. (2015), and, Ferrera-Cobos et al. (2020) observed a decrease in the ratio when the clearness index (i.e., $k_t = \mathrm{GHI}/\mathrm{E_{ext}}$) increases. In contrary, Lozano et al. (2022) found no significant dependence of the ratio on k_t. Most research studies admit that the global PAR/GHI ratio is location- and season-dependent (Hu et al., 2007; Jacovides et al., 2003; Li et al., 2010; Proutsos et al., 2022), therefore pointing out the need to further investigate the behaviour of the ratio at more sites with different climates around the globe.

The $\mathrm{PAR_{diffuse}}$ component is generally analysed by the PAR diffuse fraction (i.e., $k_{\mathrm{PAR}} = \mathrm{PAR_{diffuse}}/\mathrm{PAR_{global}}$). Several models have been proposed to obtain k_{PAR} and most of them are inspired by GHI separation models, which estimate DHI from GHI and their clearness index dependence (Gu et al., 1999; Jacovides et al., 2010; Kathilankal et al., 2014; Oliphant and Stoy, 2018; Ren et al., 2018). Since the spectral range of PAR is a portion of that of GHI, it is logically attractive to use just use GHI separation models to partition $\mathrm{PAR_{global}}$. Indeed, the recent work by Ma Lu et al. (2022) applied and evaluated several GHI separation models for separating $\mathrm{PAR_{global}}$.

Generally, empirical models based on simple mathematical expressions reported in the literature are applicable when the local conditions are similar to those used for calibrating the models. However, a limited number of studies investigate the transferability of the models to other locations around the globe. For instance, de Blas et al. (2022) analysed the accuracy of 21 semi-empirical models of $\mathrm{PAR_{global}}$ in seven locations of the SURFRAD network in the United States that the authors claimed to be representative of a large variety of weather conditions. All 21 models use a combination of easily retrievable parameters (see section 2.1 for further details). The results show that calibrating the model parameters according to the studied locations can slightly improve the estimation of the PAR components. But since the global calibrated models already offer very satisfactory results, they should be chosen considering the availability of the input variables at each specific location. These findings, nevertheless, cannot necessarily be applied to high latitudes (>49°N), and to northern European countries (e.g., northern Germany and Scandinavia)

where agrivoltaics research has expanded during the latest decade (Brodam Galacho, 2023; Mamun et al., 2022). There exists an overall lack of knowledge on the transferability and performance of PAR separation models in high-latitude environments. One of the few works carried out on PAR assessment at high latitudes was the work conducted by López et al. (2001). The latter developed a model based on artificial neural network involving only GHI and solar zenith angle, and compared it with an empirical model based on GHI, clearness index and solar zenith angle (Alados et al., 1996) in Abisko with latitude 68.35°N. However, the model was developed for PAR_{global} estimation and not $PAR_{diffuse}$.

In the work presented here, a new separation model to estimate $PAR_{diffuse}$ from PAR_{global} is proposed. It is derived from the original YANG2 model (Yang and Boland, 2019), which is a GHI separation model, because of its high accuracy demonstrated for both GHI and PAR_{global} (Ma Lu et al., 2022). In addition, the newly proposed model is based on atmospheric inputs conveniently retrievable from available databases, algorithms, and satellite-derived data. The proposed separation model is evaluated for three Integrated Carbon Observation System (ICOS) stations in Sweden, considering an evident gap in PAR separation model studies applied to northern latitudes exists and compared with the performance of four other PAR separation models. At the same time, an analysis of the seasonal trends and variation of the different PAR components is provided for these three locations.

Furthermore, the authors are currently conducting experiments on an agrivoltaic system located near Västerås, Sweden. Three further evaluations, hereafter referred as cases, of the proposed model are performed for the agrivoltaic site. The first two study cases aim to shed light on strategies to obtain the diffuse fraction of PAR from the proposed PAR separation model for any location of interest, even in the absence of in-situ PAR measurements, which is often the case. The third study case aims to provide guidance on when it is recommended to use a single-parameter separation model and when to use other more complex models.

The remainder of the study is organised as follows: Section 2 presents the meteorological data used for developing, calibrating, testing, and validating the model proposed in this study as well as the data used from the agrivoltaic site. Section 3 describes the steps taken to develop the new separation model and the methodology behind the studied cases. Section 4 evaluates the performance of the proposed model and discusses the results obtained for the selected sites. More specifically, an analysis of the fluctuations in PAR components in these high-latitude locations is presented and discussed. Additionally, the results of the three cases, showing different strategies to apply the proposed PAR separation model for agrivoltaic systems applications are analysed. Section 5 draws the conclusions of the study.

2. Weather Data

The dataset used in this work for training and testing the proposed PAR separation model consists of multiple-year measurements of PAR_{global} and $PAR_{diffuse}$ among other variables from the ICOS network in Sweden (ICOS Sweden, 2022). ICOS is a European research infrastructure, formed as a collaboration of nationally operated measurement stations. ICOS ecosystem stations follow standard protocols and requirements for all measured parameters (Carrara et al., 2018). Three locations in Sweden with available measurements were selected; namely, Lanna, Degerö, and Norunda (Figure 2). The dataset spans three years of data for each station with a time resolution of 30 min. Since the measurements of PAR from ICOS stations are in units of flux density as a quantum process (PPFD), a conversion factor of $1\,W/m^2 \approx 4.57\,\mu mol/m^2/s$ (McCree, 1972) is applied whenever required. The data for each location are divided into two subsets (Table 1). On one hand, the training set consists of two years of data, which is used to fit the separation model parameters for the site. On the other hand, the validation (or testing) set consists of the remaining one year of data, which is used to test the fitted models with unseen data for the location of concern.

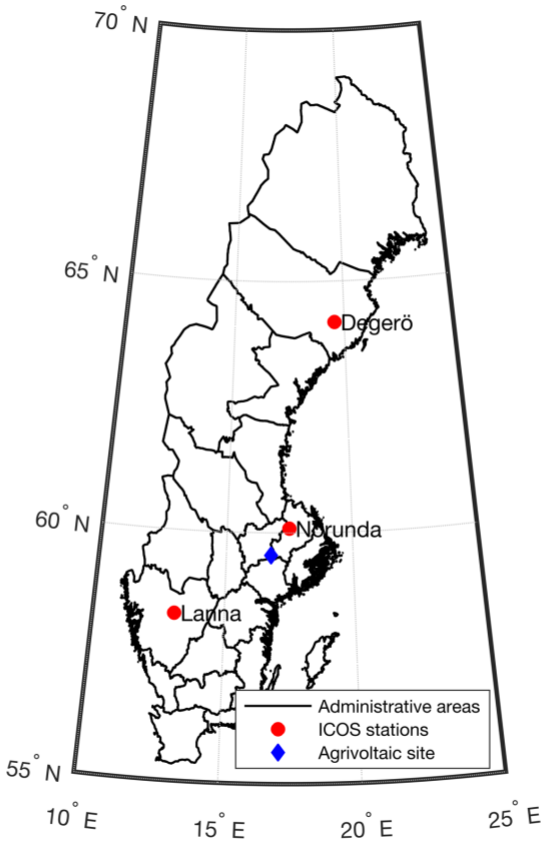

Figure 2. Map of Sweden with the location of the ICOS Sweden network stations selected for the analysis and the location of the first agrivoltaic system in Sweden. Map source: (GADM, 2022).

Table 1. Study locations and details of the data extracted from ICOS-Sweden network. The last column indicates the numbers of train/test samples (or data points) at each location after quality control (described in section 2.2) and hourly resolution.

Station	Latitude (ºN)	Longitude (ºE)	Elevation (m)	Data period	Samples training/ testing
Lanna	58º20'	13º06'	75	2016-2018	6638/ 3318
Degerö	64º18'	19º55'	270	2016- 2018	6672/ 2003
Norunda	60º05'	17º29'	46	2016-2018	5671/ 2629

2.1 Auxiliary Data

Besides $\mathrm{PAR_{global}}$ and $\mathrm{PAR_{diffuse}}$, separation models often require as input several auxiliary variables for training, which are often computable or can be accessed for general time periods and locations. These auxiliary variables are described in this section. Firstly, the extraterrestrial radiation (E_{ext}) on a horizontal plane is needed to compute k_t, is calculated as explained in Duffie & Beckman (2013). It is noted that the computation of E_{ext} requires further a parameter known as the solar constant (*SC*), which is here in taken to be $SC = 1361.1\ \mathrm{W/m^2}$, following Gueymard (2018). Moreover, the Earth's orbit eccentricity correction factor is used as per the definition by Spencer's equation (Spencer, 1971). From the eccentricity correction factor, the hour angle and thus the apparent solar time can be derived (Duffie and Beckman, 2013). Extraterrestrial PAR ($\mathrm{PAR_{ext}}$) is calculated analogously to E_{ext}, but with the approximated PAR solar constant, which is integrated from the latest synthetic extraterrestrial spectrum by Gueymard (2018) between 400 nm and 700 nm, $\mathrm{PAR_{SC}} = 531.8\ \mathrm{W/m^2}$.

The solar zenith angle is calculated from the solar elevation and the latter is derived using the solar positioning algorithm developed by Koblick (2021). Moreover, to account for the atmospheric refraction effects, the model from the ESRL Global Monitoring Laboratory (US Department of Commerce, 2021) is applied to correct the solar elevation angle. Both the clear-sky GHI ($\mathrm{G_{cs}}$) and clear-sky PAR ($\mathrm{PAR_{cs}}$) are acquired from the Clouds and the Earth's Radiant Energy System (CERES) satellite-based observations (Wielicki et al., 1996). Both satellite-derived diffuse fraction of GHI and the diffuse fraction of PAR are obtained from the CERES SYN1deg Ed. 4.1 product (Doelling, 2017). CERES offers hourly satellite-derived GHI, DHI, PAR total, and PAR diffuse from March 2000 till Dec 2022 with global coverage with a 1º x 1º spatial resolution in both latitudes and longitudes. All satellite-derived data is downloaded via the ordering portal to match the spatial locations and temporal range of the measured ICOS data.

It should be noted that even though ICOS data has a temporal resolution of 30 min (timestamp at the end of the averaging interval), due to the shortest time step availability of CERES data, which has an hourly resolution, the remaining part of this work (including both analysis and results) is performed with a 1-hour time step Coordinated Universal Time (UTC). In the present study, the half-hourly data points from ICOS

are averaged for hourly resolution. Solar zenith angle values are centred at the half of the hourly values. The metadata of the sites considered in this study is tabulated in Table 1.

2.2 Quality control

Quality control (QC) constitutes an essential part of radiation modelling, with the goal of filtering and eliminating spurious and erroneous data points. Since the observational data are to be used for the determination of fitting parameters, validation, and performance comparison of the separation models, QC must be applied to ensure that exclusively the highest-quality data points are selected. That said, there is no ideal or universally accepted QC procedure for broadband irradiance data, not to mention PAR data. This issue has been pointed out in the introduction section and in the previous work by Ma Lu et al. (2022). On that account, the previously used QC procedure for PAR is adopted for this work as well. The reader is referred to the previous publication for a detailed list of quality filters both dealing with solar angles and radiation (Ma Lu et al., 2022). The only added quality filter corresponds to albedo for which data with values greater than one was rejected.

2.3 Agrivoltaic site data

The dataset used for the additional cases at the agrivoltaic site near Västerås (59.55°N, 16.76°E), Sweden (Figure 3), comprises in-situ PAR_{global} and $PAR_{diffuse}$ measurements taken from April to December 2022. These PAR measurements were recorded at a 1-minute time resolution using a Delta T BF5 Sunshine Sensor, equipped with an array of photodiodes and a computer-generated shadow mask. The hourly

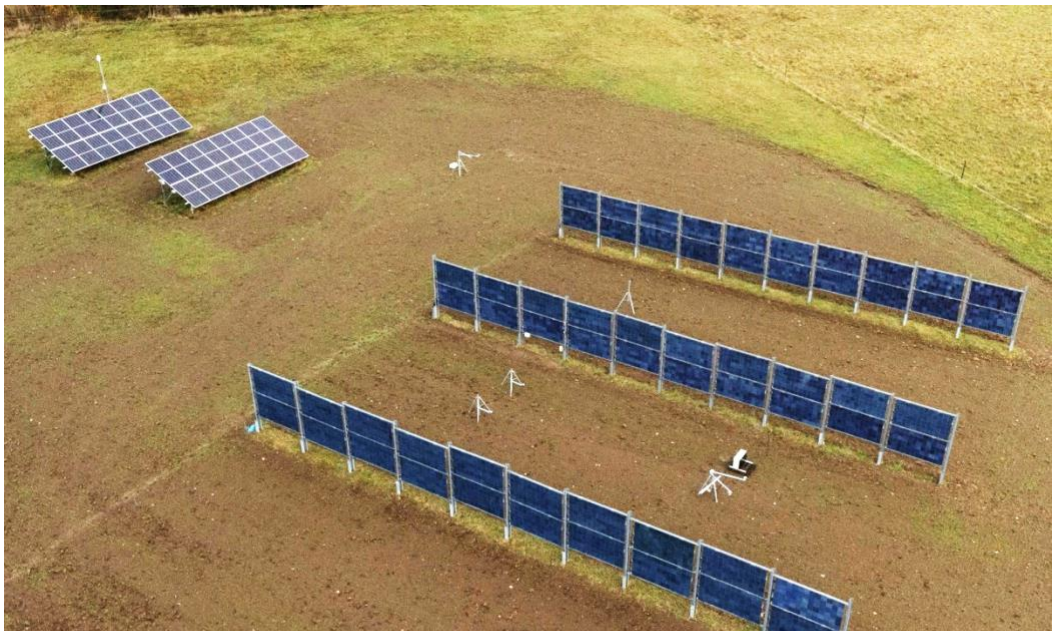

Figure 3. Aerial picture of the first agrivoltaic system in Sweden comprising of three vertical bifacial PV rows. Photo credit: IVAR Studios AB.

averaged PAR measurements are used to calculate the in-situ PAR diffuse fraction, which is then compared to the predicted $PAR_{diffuse}$ fraction from the proposed model.

In the first case, all the input parameters required for the proposed model are derived from available databases, specifically CERES (Doelling, 2017) and ERA5 (Hersbach et al., 2023). For the second and third cases, the input parameters used to feed the proposed model are based on a combination of in-situ measurements and satellite-derived databases, Further information is outlined in section 3.5, Table 2.

The in-situ measurements to feed the models are logged at a 1-minute time resolution but are averaged to an hourly temporal resolution for this study. These measurements include global horizontal irradiance (GHI) and diffuse horizontal irradiance (DHI) obtained from a Delta T SPN1 Sunshine Pyranometer, as well as air temperature and relative humidity data from a Lufft WS600-UMB Smart Weather Sensor, and albedo data from an Apogee SP-710-SS Albedometer. All in-situ measurements and satellite-derived parameters have undergone quality checks, as described in section 2.2, and have been averaged to an hourly temporal resolution.

3. Methodology

The proposed PAR separation model is derived from the original GHI separation model YANG2 (Yang and Boland, 2019), which has been identified in previous work as the most accurate PAR separation model (Ma Lu et al., 2022). YANG2 itself is an adaptation of the Boland-Ridley-Lauret (BRL) (Ridley et al., 2010) logistic form GHI separation model. As a result, the proposed model also follows the logistic form but incorporates additional predictors beyond those used in YANG2. These additional predictors have been carefully selected through a literature review, as presented in the section 3.1. Utilising these new predictors, the new PAR separation model is constructed (section 3.2), and the significance and coefficient estimates for these predictors are determined for the three ICOS stations via nonlinear regression (section 3.3). To assess the performance of the proposed PAR separation model, four other existing PAR separation models are evaluated for the studied locations, and their results are compared using common statistical indicators for model assessment (section 3.4). A graphical representation of the methodology is provided in Figure 4.

Furthermore, the paper outlines three cases (section 3.5) that demonstrate different strategies and applications of PAR separation models to obtain the diffuse PAR fraction in situations where $PAR_{diffuse}$ is not directly measured in-situ. Such scenarios are common, but they have gained increased interest, especially for agrivoltaic systems modelling as illustrated at the agrivoltaic site near Västerås.

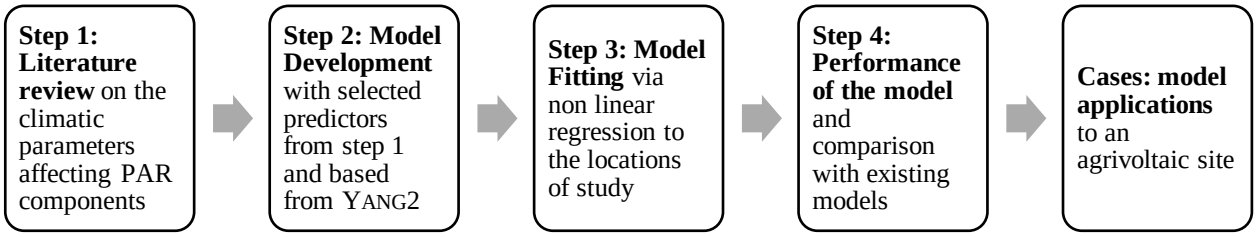

Figure 4. Schematic diagram of the workflow applied in this work for the development of a new PAR separation model.

3.1 Literature review on the climatic parameters affecting the diffuse component of photosynthetically active radiation

An initial literature review has been performed to analyse which atmospheric variables most influence the ecosystem production efficiency and, thus, the PAR components.

In the study by Li et al. (2020), in a desert steppe ecosystem, lower vapour pressure deficit (VPD ≤ 1 kPa), lower air temperature (Ta < 20°C) and non-stressed water conditions were more favourable conditions for enhanced ecosystem photosynthesis under cloudy skies ($k_t < 0.7$). $\mathrm{PAR_{diffuse}}$ peaked when k_t was around 0.5.

A work by Lu et al. (2022) using data from 40 sites around the globe has concluded that VPD and soil moisture (SM) are significant variables in ecosystem production efficiency that should be fairly valued in ecosystem modelling. For most of the studied sites, high VPD values cause positive changes in PAR while low SM values cause negative changes in the fraction of PAR absorbed by the plants (fPAR). The study underlines the influence of VPD on incident PAR in a multitude of locations. Yet none of those sites was in northern latitudes.

A new method to estimate PAR values for clear-sky conditions used solar zenith angle, total column contents of ozone (TOC) and water vapour (TWV), aerosol optical depth (AOD), vertical profiles of temperature, pressure, density and volume mixing ratio of gases, elevation and ground albedo as inputs (Wandji Nyamsi et al., 2019). The study emphasised that the errors in the suggested method were caused by the overestimation of the input variables AOD and the assumption of constant $\mathrm{PAR_{albedo}}$, suggesting these two variables have a significant effect on the PAR under clear skies.

Recent work by de Blas et al. (2022), analysed $\mathrm{PAR_{global}}$ estimations at 1-min, hourly, and daily time steps at seven sites from 21 models that use a combination of the following meteorological parameters: GHI, clearness index, diffuse fraction, vapour pressure, relative optical air mass, precipitable water, solar zenith angle, sky brightness, and sky clearness. The work further analysed the performance of the models for

different groups of sky conditions (clear to overcast) and found that for some models, the accuracy worsened when applied to overcast skies.

Another recent work by Proutsos et al. (2022) studied the atmospheric factors affecting the PAR/GHI ratio in a Mediterranean site. The authors concluded that the atmospheric water content (expressed by the degree of cloudiness, actual water vapour, optical thickness, or dew point temperature) and the clearness index were the most influential factors in the ratio. Air temperature and related meteorological variables (relative humidity, vapour pressure deficit and saturation vapour pressure) were found to have no significant effect on the ratio.

Regarding PAR diffuse estimations, the latest work by Lozano et al. (2022) found a clear dependence of the k_{PAR} on the clearness index and total cloud cover (TCC) at a Mediterranean site. The authors proposed a model to estimate k_{PAR} obtained through the first adaptation of the Boland-Ridley-Lauret (BRL) model (Ridley et al., 2010) based on the PAR clearness index, solar elevation angle, apparent solar time (AST), daily PAR clearness index and persistence index. When fitting the model to the studied site, the authors found that AST and daily PAR clearness index were insignificant and suggested these terms be removed from the model.

Kathilankal et al. (2014) developed a semi-parametric PAR separation model for the United States. It adapts the BRL model using physically viable climate variables as predictors: relative humidity, PAR clearness index, surface albedo and solar elevation angle. The proposed model takes a conditional approach, which uses two logistic fits: one for clear-sky conditions and the other for cloudy conditions.

Based on the literature, the parameters VPD, AOD, optical thickness, relative humidity, and albedo are not included in the YANG2 model, but appear to influence $\mathrm{PAR}_{\mathrm{diffuse}}$. In addition, their values can be retrieved with relative ease.

3.2 Model development

YANG2 (Yang and Boland, 2019), which is a logistic form model, has been selected as the starting point for developing the new PAR separation model. The logistic form is chosen based on the agreement in the literature as yielding higher accuracy for both for separation models of GHI and separation models of PAR in comparison with other functional shapes. Previous work by Ma Lu et al. (2022) showed that YANG2 and STARKE (Starke et al., 2018) were among the best-performing models to obtain $\mathrm{PAR}_{\mathrm{diffuse}}$ from $\mathrm{PAR}_{\mathrm{global}}$. It should be noted that both YANG2 (Eq.1) and STARKE (Eq.4) were originally developed for decomposing GHI by estimating the diffuse fraction, $k = \frac{\mathrm{DHI}}{\mathrm{GHI}}$. For this reason, Ma Lu et al. (2022) have applied the Spitters relationship (Eq.6) (Spitters et al., 1986) to expand the applicability of these models to PAR separation.

$$k^{\text{YANG2}} = C + \frac{1 - C}{1 + e^{\beta_0 + \beta_1 k_t + \beta_2 \text{AST} + \beta_3 Z + \beta_4 \Delta k_{tc} + \beta_6 k^{(s)}}} + \beta_5 k_{de}, \tag{1}$$

$$\Delta k_{tc} = k_{tc} - k_t = \frac{G_{\text{cs}}}{E_{\text{ext}}} - k_t, \tag{2}$$

$$k_{de} = \max\left(0, 1 - \frac{G_{\text{cs}}}{\text{GHI}}\right), \tag{3}$$

$$k^{\text{STARKE}} = \begin{cases} \dfrac{1}{1 + e^{\beta_7 + \beta_8 k_t + \beta_9 \text{AST} + \beta_{10} Z + \beta_{11} K_T + \beta_{12} \psi + \frac{\beta_{13} G_{\text{cs}}}{277.78}}}, k_{\text{CSI}} \geq 1.05 \text{ and } k_t > 0.65; \\ \dfrac{1}{1 + e^{\beta_0 + \beta_1 k_t + \beta_2 \text{AST} + \beta_3 Z + \beta_4 K_T + \beta_5 \psi + \frac{\beta_6 G_{\text{cs}}}{277.78}}}, \text{otherwise} \end{cases} \tag{4}$$

$$K_T = \frac{\sum_{n=1}^{24} \text{GHI}_n}{\sum_{n=1}^{24} E_{\text{ext}_n}}, \tag{5}$$

$$k_{\text{PAR}}^{\text{model}} = \frac{\text{PAR}_{\text{diffuse}}}{\text{PAR}_{\text{global}}} = \frac{\left[1 + 0.3\left(1 - (k^{\text{model}})^2\right)\right] k^{\text{model}}}{1 + (1 - (k^{\text{model}})^2) \cos^2(90 - \beta) \cos^3 \beta} \tag{6}$$

Briefly, k_t is the clearness index, G_{cs} is the clear-sky GHI [W/m^2], Z is the solar zenith angle [°], AST is the apparent solar time [h], E_{ext} is the extraterrestrial radiation [W/m^2], $k^{(s)}$ is the satellite-derived diffuse fraction, K_T is the daily clearness index, the ψ predictor is the three-point moving average of clearness index, k_{CSI} is the clear-sky index, and β is the solar elevation angle [°]. To avoid repetition, the reader is directed to the original model's publications for a comprehensive explanation of the parameters' physical significance. C and $\beta_0, \ldots, \beta_{13}$ are the coefficients of the model. The superscript "model" in k^{model} and $k_{\text{PAR}}^{\text{model}}$ indicates the applicable separation model, for instance YANG2 or STARKE.

In the present work, the model form of YANG2 is taken as a basis. The following model (Eq. 7), hereafter called CLY (i.e., an abbreviation of the main developers' family names in alphabetical order), is proposed by including four new relevant variables, i.e., albedo, optical thickness, AOD and VPD, derived from the literature review. Relative humidity was not considered due to its high correlation with VPD (Eq. 10 and Eq.11).

$$k^{\text{CLY}} = C + \frac{1 - C}{1 + e^{\beta_0 + \beta_1 k_t + \beta_2 \text{AST} + \beta_3 Z + \beta_4 \Delta k_{tc} + \beta_5 \alpha + \beta_6 \tau + \beta_7 \text{AOD} + \beta_8 \text{VPD} + \beta_{10} k^{(s)}}} + \beta_9 k_{de}, \tag{7}$$

$$\tau = \ln\left(\frac{E_{ext}}{BHI}\right) \frac{1}{AM} \tag{8}$$

$$\text{AM} = \frac{1}{\cos(Z) + 0.50572 * \left(6.07995 + (90 - Z)\right)^{-1.6364}} \tag{9}$$

$$\text{VPD} = e_s - e_a \tag{10}$$

$$e_a = e_s * \frac{\mathrm{RH}}{100} \tag{11}$$

$$e_s = 6.1078 * \exp\left(\frac{17.27 * Ta}{Ta + 237.3}\right) \tag{12}$$

Here, α is the surface albedo, τ is the optical thickness calculated according to the Beer-Lambert Law (Ineichen, 2008), BHI is the beam or direct horizontal irradiance [W/m^2], AM is the air mass calculated using the definition by Kasten & Young (1989), AOD is the aerosol optical depth at 550 nm, VPD is the vapour pressure deposition [mbar], e_a is the actual vapour pressure [mbar] and e_s is the saturation vapour pressure [mbar], both calculated according to the Technical Committee on Standardization of Reference Evapotranspiration (2005), RH is the relative humidity and T_a is the ambient temperature. Similarly, C and $\beta_0, \ldots, \beta_{10}$ are the coefficients of the model.

To obtain the diffuse fraction of PAR using the proposed model, Eq. 6 should likewise be applied to Eq.7. $k_{\mathrm{PAR}}^{\mathrm{CLY}}$ is obtained as follows:

$$k_{\mathrm{PAR}}^{\mathrm{CLY}} = \frac{[1 + 0.3(1 - (k^{\mathrm{CLY}})^2)]k^{\mathrm{CLY}}}{1 + (1 - (k^{\mathrm{CLY}})^2)\cos^2(90 - \beta)\cos^3\beta} \tag{13}$$

CLY is evaluated for the three selected ICOS network stations (described in Section 2), and its performance compared to that of the original YANG2 and STARKE models, in addition to two other PAR separation models mentioned in the literature review. These additional PAR separation models adapt the BRL logistic form model with distinct predictors and were developed to provide k_{PAR} without the need to implement the relationship outlined in Eq. 6. Kathilankal et al. (2014) and Lozano et al. (2022) proposed these models, hereafter called KATHILANKAL (Eq.14) and LOZANO (Eq.16) respectively:

$$k_{\mathrm{PAR}}^{\mathrm{KATHILANKAL}} = \begin{cases} \dfrac{1}{1 + e^{-(\beta_0 + \beta_1 k_{t\_\mathrm{PAR}} + \beta_2 \mathrm{RH} + \beta_3 \alpha + \beta_4 \sin(\beta))}}, & k_{t\_\mathrm{PAR}} \leq 0.78; \\ \dfrac{1}{1 + e^{-(\beta_5 + \beta_6 k_{t\_\mathrm{PAR}} + \beta_7 \mathrm{RH} + \beta_8 \alpha + \beta_9 \sin(\beta))}}, & k_{t\_\mathrm{PAR}} > 0.78 \end{cases} \tag{14}$$

$$k_{t\_\mathrm{PAR}} = \frac{\mathrm{PAR}_{\mathrm{global}}}{\mathrm{PAR}_{\mathrm{ext}}} \tag{15}$$

$$k_{\mathrm{PAR}}^{\mathrm{LOZANO}} = \frac{1}{1 + e^{\beta_0 + \beta_1 k_{t\_\mathrm{PAR}} + \beta_2 \beta + \beta_3 \mathrm{AST} + \beta_4 K_{T\_\mathrm{PAR}} + \beta_6 \psi_{\mathrm{PAR}}}} \tag{16}$$

$$K_{T\_\mathrm{PAR}} = \frac{\sum_{n=1}^{24} \mathrm{PAR}_{\mathrm{global}_n}}{\sum_{n=1}^{24} \mathrm{PAR}_{\mathrm{ext}_n}}, \tag{17}$$

where k_{t_PAR} is the clearness index of PAR, K_{T_PAR} is the daily clearness index of PAR and ψ_{PAR} is the persistence index defined as the two-point moving average of the clearness index of PAR. Similarly, $\beta_0, \ldots, \beta_9$ are the coefficients of the models.

3.3 Model fitting

The coefficients of predictors for the proposed model CLY and the four other models (YANG2, STARKE, KATHILANKAL and LOZANO) are estimated using non-linear regression least squares fit with Matlab R2023a built-in function *fitnlm* (MathWorks, 2023). The datasets used to estimate the coefficients of the models are the training datasets enumerated in Table 1 for the three study locations. The choice of a least squares fit aligns with the statistical concept of consistency (Gneiting, 2011), given that one of the primary evaluation metrics is the normalised root mean square error (section 3.4). Prior research on the calibration and evaluation of point forecasts has emphasised the concept of consistency (Yang et al., 2020; Yang and Kleissl, 2022).

The algorithm for non-linear regression estimates model coefficients using an iterative procedure beginning with initial values. The initial values for the four existing models are derived from the models' original publications, whereas the initial values for the proposed model are similar for the predictors appearing in the YANG2 model and 0 for the new predictors. The maximum number of permitted iterations and other parameters (such as tolerances) are left at their default values (MathWorks, 2023).

3.4 Model evaluation metrics

The performance of the proposed CLY model (Eq.7) is evaluated with the testing datasets at the different sites introduced in Section 2 by employing several popular error metrics. The results are then compared to the performances of four other models described in Section 3.2 at the same studied locations.

The error metrics selected in this work are the same ones utilised by Ma Lu et al. (2022): the normalised mean bias error (nMBE), the normalised root mean square error (nRMSE), and the coefficient of determination (R^2). The observations of k_{PAR} are derived from the measurements of $\mathrm{PAR}_{\mathrm{global}}$ and $\mathrm{PAR}_{\mathrm{diffuse}}$ at the studied ICOS stations. The predictions are the $k_{\mathrm{PAR}}^{\mathrm{model}}$ calculated from the models (i.e., CLY, YANG2, STARKE, KATHILANKAL and LOZANO).

3.5 Model application cases

Three different cases are considered for the application of the proposed PAR separation model in agrivoltaic systems. Although these cases utilise the CLY model, the approaches are valid for any existing separation models provided that the required parameters and data are known.

In the first case (**Case 1**), the agrivoltaic system's location is known, but there are no in-situ measurements nor nearby weather station data available to feed the model. The approach involves using input data solely from available satellite-derived databases for the proposed PAR separation model. The CLY model applied in this case is calibrated using the combined measured training data from the three ICOS network stations described in Section 2 Table 1. The accuracy of this approach is then compared to in-situ measurements of the diffuse fraction of PAR at the agrivoltaic site, as described in Section 2.3, located near Västerås, Sweden. The required input data for the CLY model's predictors in this specific scenario are gathered as outlined in Table 2.

In the second case (**Case 2**) the proposed CLY model, calibrated using the combined measured data from the three Swedish ICOS network stations studied previously, is also applied to the agrivoltaic site in Västerås. However, in this case, the input data required by the CLY model are assumed to be known (i.e., measured in-situ) (Table 2). Similarly, the accuracy of this second approach is compared to the in-situ measurements of the diffuse fraction of PAR.

The third case (**Case 3**) follows a similar model validation approach as with the studied ICOS stations. It assumes that all the required data to run the model at the agrivoltaic site are known, including the PAR diffuse for a specific period (Table 2). The model is calibrated using 2/3 of the available measured data, which includes the in-situ measurements of the diffuse fraction of PAR, and then tested with the remaining unseen data (1/3 of the available measured data). The same testing data is also used with the ERBS single-parameter separation model of GHI (Eq.18) with the Spitters relationship (Eq.6) to obtain the diffuse fraction of PAR. ERBS has been used in a previous agrivoltaic study to determine the $PAR_{diffuse}$ component (Willockx et al., 2020) and is also incorporated into PV modelling tools such as *pvlib* (F. Holmgren et al., 2018) and PVsyst for obtaining the DHI from GHI. Additionally, the same testing data is used for the CLY model using the coefficients from the combined ICOS sites (as in Case 1 and Case 2). The performances of the CLY model calibrated to in-situ measurements, CLY model calibrated to the three ICOS network stations, and the ERBS model are then compared using the same indicators as in section 3.4. The objective of this comparison is to highlight that simple GHI separation models like ERBS can be directly applied to decompose PAR (Ma Lu et al., 2022). However, caution must be exercised as the value of the diffuse fraction of GHI does not necessarily equal the value of the diffuse fraction of PAR (the Spitters relationship, Eq.6, should be considered). Additionally, it is possible that the one-parameter ERBS model is overly simple and fails to accurately represent the true distribution of the data. Another goal is to illustrate the differences between using the calibrated CLY model especially for the location under investigation or utilising a broad calibration derived from other stations within the same country.

$$k^{\text{ERBS}} = \begin{cases} 1.0 - 0.09k_t, & k_t \leq 0.22 \\ 0.9511 - 0.1604k_t + 4.388k_t^2 - 16.638k_t^3 + 12.336k_t^4, & 0.22 < k_t \leq 0.80 \\ 0.165, & k_t > 0.80 \end{cases} \quad (18)$$

Table 2 details the input data sources used for the CLY model in the various examined cases, as well as the primary analysis performed for the three ICOS network stations. This table summarizes for the reader the data sources utilised for each analysis.

Table 2. Datasets used to obtain the predictor values of the proposed PAR separation model (CLY) for each of the cases under study. The Main Analysis column refers to the data used for developing, training and testing the proposed model in three distinct Swedish ICOS network stations. Case 1 to 3 are the studies located in the agrivoltaic (AV) site close to Västerås, Sweden.

Predictor (Sub-variables)[a]	**Main Analysis (Lanna, Degerö, Norunda)**	**Case 1 (AV site)**	**Case 2 (AV site)**	**Case 3 (AV site)**
k_t ($\mathbf{GHI}, E_{ext}$[b])	ICOS ("ICOS Sweden," 2022)	CERES (Doelling, 2017)	Own measurements Section 2.3	Own measurements Section 2.3
AST	As described in Section 2.1(Duffie and Beckman, 2013)	As described in Section 2.1(Duffie and Beckman, 2013)	As described in Section 2.1(Duffie and Beckman, 2013)	As described in Section 2.1(Duffie and Beckman, 2013)
$\boldsymbol{Z}$	As described in Section 2.1(Koblick, 2021)	As described in Section 2.1(Koblick, 2021)	As described in Section 2.1(Koblick, 2021)	As described in Section 2.1(Koblick, 2021)
Δk_{tc} ($\boldsymbol{G_{cs}}, E_{ext}$[b], k_t)	CERES (Doelling, 2017)	CERES (Doelling, 2017)	CERES (Doelling, 2017)	CERES (Doelling, 2017)
$\boldsymbol{\alpha}$	ICOS[c] ("ICOS Sweden," 2022)	CERES (Doelling, 2017)	Own measurements Section 2.3	Own measurements Section 2.3
τ (E_{ext}[b], **BHI**, AM[d])	CERES (Doelling, 2017)	CERES (Doelling, 2017)	Own measurements Section 2.3	Own measurements Section 2.3
AOD	CAMS-AOD[e] (ECMWF, 2022)	CERES (Doelling, 2017)	CERES (Doelling, 2017)	CERES (Doelling, 2017)
VPD (**RH**, **Ta**)	ICOS ("ICOS Sweden," 2022)	ERA5[f] (Hersbach et al., 2023)	Own measurements Section 2.3	Own measurements Section 2.3
$k^{(s)}$ (**GHI**, **DHI**)	CERES (Doelling, 2017)	CERES (Doelling, 2017)	CERES (Doelling, 2017)	CERES (Doelling, 2017)
k_{de} ($\boldsymbol{G_{cs}}$, **GHI**)	Same as for k_t and Δk_{tc}	Same as for k_t and Δk_{tc}	Same as for k_t and Δk_{tc}	Same as for k_t and Δk_{tc}

[a]The sub-variables required to obtain the value of the predictor are between parentheses. In **bold** are the variables where the sources of the table refer to.
[b] $\boldsymbol{E_{ext}}$ is obtained as described in section 2.1.
[c] Albedo is calculated from ICOS parameters as the ratio of outgoing shortwave radiation / incoming shortwave radation from a net radiometer. For Norunda station, the albedo trend was dubious, and the predictor was initially insignificant (p-value > 0.05) when calibrating the model. Hence, CERES-derived albedo was instead used for Norunda.

[d] AM is obtained as defined in Eq.9.
[e]AOD 550 nm from CAMS-AOD satellite-derived service provided by ECMWF has a time step of 3h. Shape-preserving piecewise cubic interpolation is used to achieve hourly data.
[f]ERA5 dataset provides air temperature (Ta) and dew point temperature (Td). Actual vapor pressure (e_a) can be derived from Td similarly as saturation vapor pressure (e_s) from Ta (Eq.12), since RH and Td are related (Barenbrug, 1974).

4. Results and discussion

4.1 CLY separation model performance

The proposed CLY separation model for estimating diffuse PAR is evaluated alongside four other models at the three ICOS network stations, using hourly analysis and the performance metrics presented in Section 3.4. These include YANG2, STARKE, KATHILANKAL and LOZANO as described in Section 3.2. Table 3 presents the models' performances.

Table 3. The nRMSE [%], nMBE [%] and R^2 in predicted hourly diffuse PAR from of the proposed PAR separation model, CLY, compared to other 4 models. Locally fitted coefficients (using training data over 2-years, period 2016-2017) and validated (using testing data over 1-year, period 2018) at 3 ICOS-Sweden stations (Lanna, Degerö, Norunda). The errors are computed between the predicted and measured hourly PAR diffuse fraction values. Boldface denotes the best-performing model in a row.

Station	CLY	YANG2	STARKE	KATHILANKAL	LOZANO
nRMSE [%]					
Lanna	**12.58**	13.25	14.31	24.33	16.28
Degerö	**18.23**	18.62	20.28	21.61	19.67
Norunda	**15.71**	16.27	17.42	20.44	17.00
nMBE [%]					
Lanna	-3.23	-1.97	-3.10	2.91	**-1.36**
Degerö	-1.10	**0.37**	-1.8	1.21	-2.56
Norunda	-2.35	-1.75	-2.93	**0.33**	-1.45
R^2					
Lanna	**0.94**	0.93	0.92	0.77	0.90
Degerö	**0.90**	0.89	0.87	0.85	0.88
Norunda	**0.92**	0.91	0.90	0.86	0.90

The CLY model demonstrates superior accuracy in terms of nRMSE and R^2 compared to the other investigated models for all locations. The additional predictors in the CLY model, namely optical thickness, vapour pressure deficit, aerosol optical depth, and surface albedo, enable a better representation of the scattered processes in the atmosphere compared to the other models. Particularly, the CLY model effectively estimates the shape of the envelope and the larger spread of data, as observed in Figure 5 . On the other hand, separation models with fewer predictors (i.e., KATHILANKAL and LOZANO) have thinner envelopes, which limits their ability to illustrate all possible combinations of diffuse PAR fraction for the same clearness index observed in the measured data, leading to lower accuracy.

Furthermore, the KATHILANKAL model, originally developed for the United States and based on data from several locations in the country (including one high-latitude location at 68.99°N), exhibited increased errors for lower solar elevation angles (common at higher latitudes). This could explain the lower accuracy obtained for the KATHILANKAL model in this study when compared to the others. During the literature review, the authors of LOZANO model discovered that when fitting the model to their studied site at a latitude of 37.16°N, AST and daily PAR clearness index were deemed insignificant and proposed to remove them. However, this trend is not observed for the studied high-latitude locations, as the p-values obtained for these coefficients were indeed significant (Table 4). This highlights the importance of model calibration and the varying impact of predictors at different latitudes and climates.

In a previous study by Ma Lu et al. (2022), the performances of the YANG2 and STARKE models performances were found to be among the leading ones. The CLY model slightly outperforms these two thanks to the added predictors, and the non-linear regression model fitting resulted in all coefficients being significant (p-value < 0.05) for the investigated locations (Table 4). This finding aligns with the observations during the literature review stage regarding the influence of these additional predictors on $PAR_{diffuse}$.

Table 4. Model coefficients of the proposed CLY PAR separation model fitted via non-linear regression least-squares method to the 3 ICOS stations in Sweden with hourly time step (Lanna, Degerö, and Norunda) each with 2 years of data corresponding to the period 2016-2017. In parentheses are the p-values.

Station	C	β_0	β_1	β_2	β_3	β_4	β_5	β_6	β_7	β_8	β_9	β_{10}
Lanna	0.1004 (0.000)	0.7564 (0.000)	4.7632 (0.000)	-0.1303 (0.000)	0.0032 (0.016)	-2.4211 (0.000)	-1.2458 (0.000)	-0.0712 (0.001)	-1.1196 (0.000)	0.0381 (0.000)	0.2390 (0.000)	-1.7076 (0.000)
Degerö	0.1038 (0.000)	-1.8417 (0.000)	5.6991 (0.000)	-0.0469 (0.000)	0.0121 (0.000)	-2.1593 (0.000)	-0.5655 (0.000)	-0.1437 (0.000)	-0.6445 (0.000)	0.0622 (0.000)	0.7358 (0.000)	-1.4455 (0.000)
Norunda	0.0841 (0.000)	-1.1836 (0.000)	5.6424 (0.000)	-0.0959 (0.000)	0.0075 (0.000)	-2.0551 (0.000)	-0.5010 (0.037)	-0.1674 (0.000)	-1.2362 (0.000)	0.0469 (0.000)	-1.0363 (0.000)	0.5121 (0.000)

Despite having several predictors, the proposed model is widely applicable thanks to the availability of satellite-derived data products (e.g., CERES (Doelling, 2017), MODIS (Schaaf and Wang, 2021), CAMS (ECMWF, 2022)). However, it is essential to acknowledge that satellite-derived data have limitations in terms of both low spatial resolution and temporal resolution (Yagli et al., 2020). Therefore, when conducting site assessments for smaller areas or regions with diverse topography and significant variation

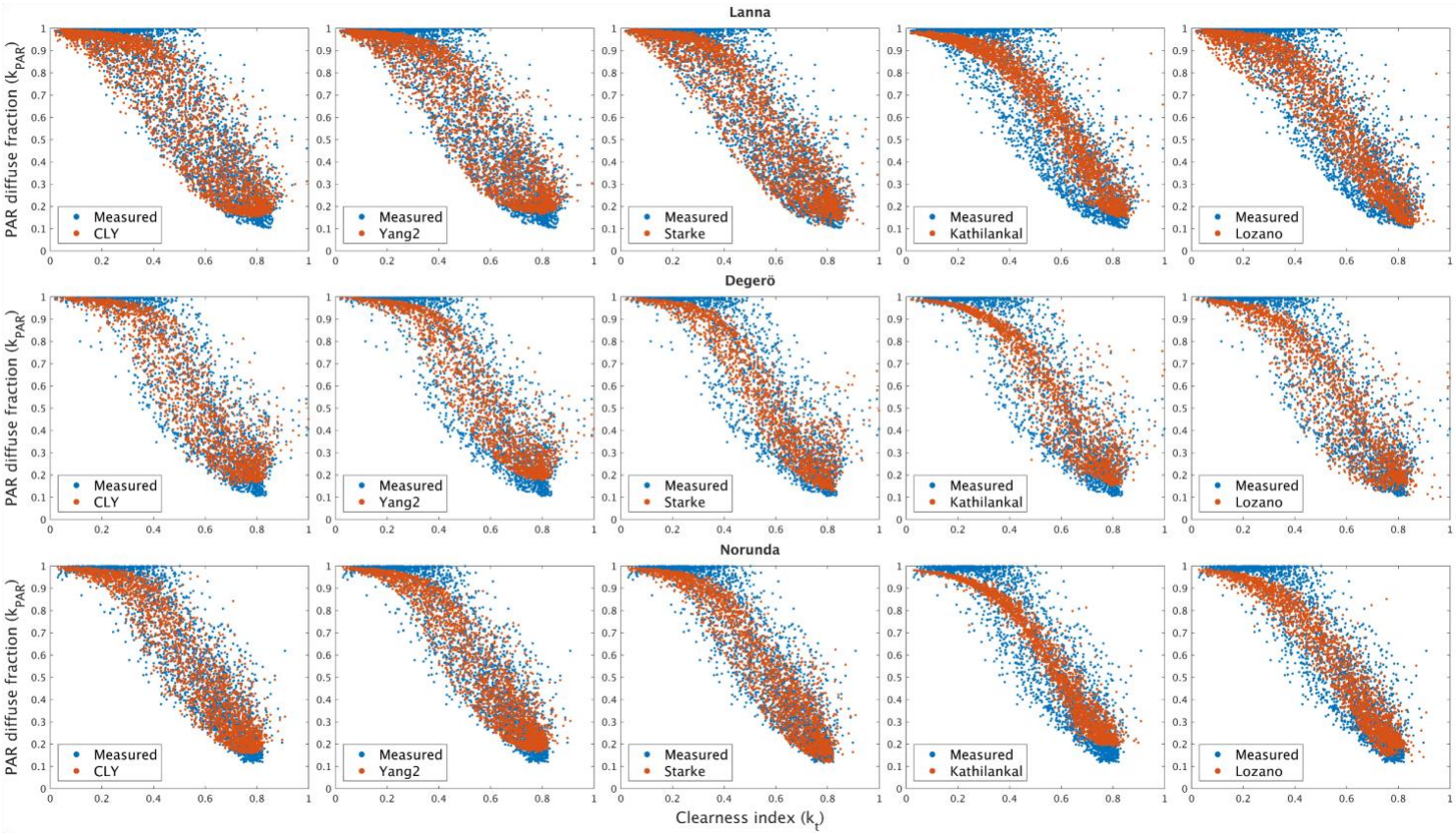

Figure 5. PAR diffuse fraction measured data plotted against the clearness index for the studied locations: Lanna (top row), Degerö (middle row), and Norunda (bottom row). The estimated results from the proposed PAR separation model CLY, YANG2, STARKE, KATHILANKAL and LOZANO are overlaid. The total number of data points in each plot refers to the testing data sample listed in Table 1.

in climate conditions, caution must be exercised when relying solely on satellite-derived data. The results obtained may reflect the average conditions of the entire pixel area covered by the satellite data, rather than the specific characteristics of the studied area. To ensure more accurate results, it is preferable to incorporate as many in-situ measurements as possible as predictor values for the model. To explore the application of the proposed CLY PAR separation model in the agrivoltaic sector under different data availability scenarios, three further analyses are performed on an actual agrivoltaic site with in-situ measurements of PAR diffuse fraction. The results of these analyses are presented further in section 4.3. Prior to that, to address the lack of studies on PAR components, particularly in high-latitude regions, the seasonal trends and variations of the various PAR components for the three investigated locations are examined in the

subsequent section. This analysis seeks to shed light on the behaviour of PAR in regions with higher latitudes.

4.2 Photosynthetically active radiation components variation at northern latitudes

As highlighted in the introduction, studies on the behaviour of PAR components for high-latitude regions are lacking. The annual evolution for PAR_{global}, PAR_{direct} and $PAR_{diffuse}$ measured at the ICOS sites at the three study locations is depicted in Figure 6. The monthly distribution of PAR_{global} shows a clear cycle, with maximum mean and median values around May and July for all locations, and the lowest values during winter. This seasonality trend is similarly observed in other studies for the northern hemisphere, such as the study by Lozano et al. (2022) in Granada, Spain (37.16° N, 3.61° W). However, the magnitude of PAR_{global} differs. In the Mediterranean location, the PAR_{global} during the warmest months exhibited values higher than 250 W/m^2, while the maximum in the Scandinavian sites was around 150 W/m^2 (with the exception of 2018, which reached average values slightly below 200 W/m^2). Moreover, the Lanna station, located at the southernmost latitude, received on average 30.64% more annual PAR_{global} radiation than Degerö, located 6° further north, for the period 2016-2017.

The seasonal pattern of the PAR_{direct} component exhibits the highest variation and distribution. The direct component is clearly influenced by the Sun's position and the intensity of the incoming light. It is worth noting that 2016 and 2017 present similar distributions, while 2018 shows a significantly different distribution. The atypical behaviour is aligned with the drought that occurred in Sweden in 2018. The country experienced an earlier onset of summer at the start of May, which lasted throughout the summer months, with short interruptions mainly in June (Wilcke et al., 2020). For the three locations investigated, the average PAR_{direct} value was 57.48% higher in May 2018 than in the previous two years. The increased solar irradiance in 2018 was caused by the anomalous presence of clear sky conditions (Räisänen, 2019; Sinclair et al., 2019).

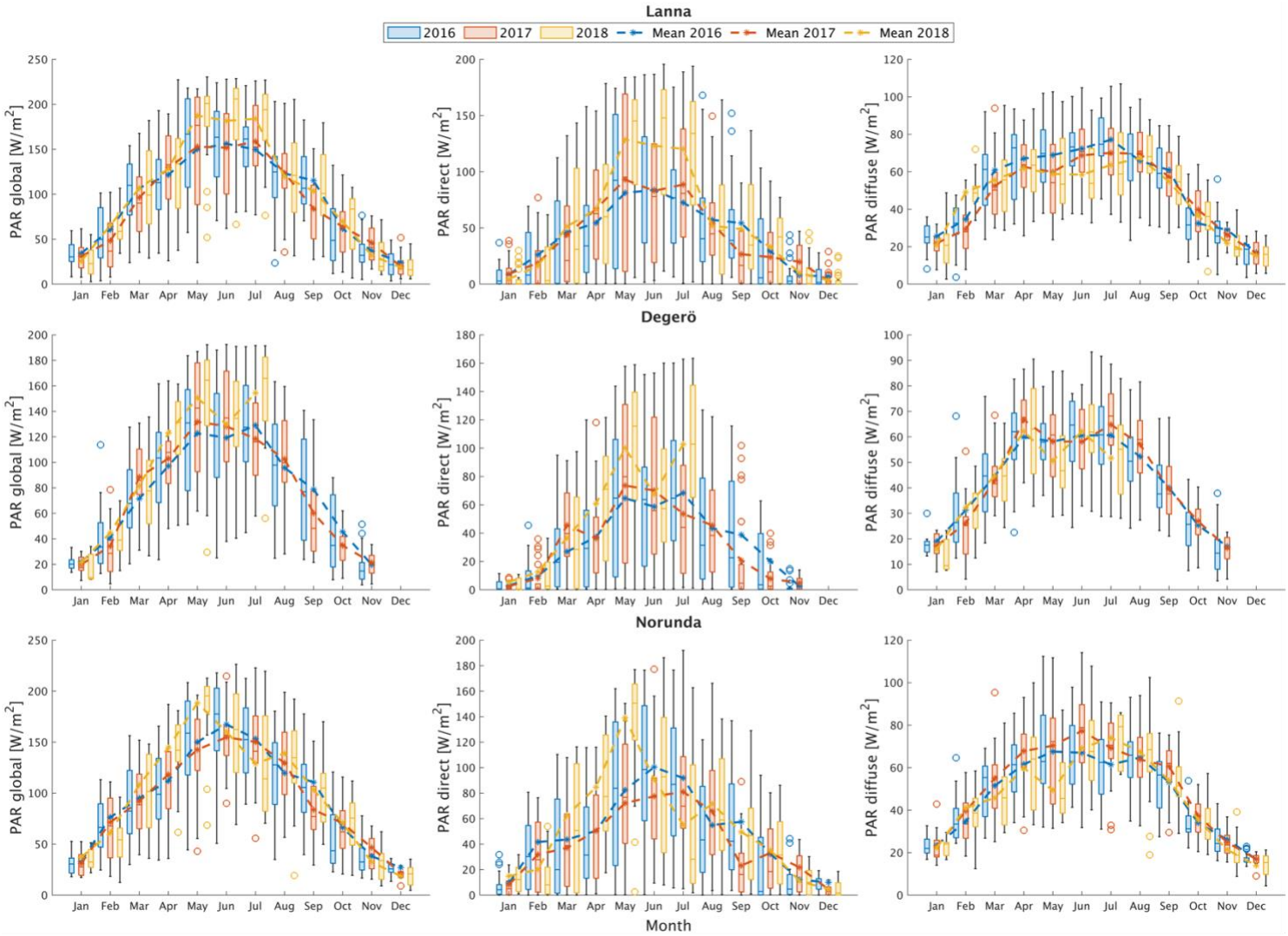

Figure 6. Monthly variation statistics for PAR_{global}, PAR_{direct} and $PAR_{diffuse}$ during the period 2016 – 2018 at the studied ICOS Sweden network stations: Lanna (top), Degerö (middle), and Norunda (bottom). For each box, central lines are the median, and upper and lower limits represent the percentiles 75th and 25th respectively. The limits of the segments represent the minimum and the maximum daily average values. The stars are the mean monthly values.

The monthly variation observed in Figure 6 for $PAR_{diffuse}$ is less pronounced than for PAR_{direct} or PAR_{global}. The main reason is the high complexity of the scattering processes involved in the diffuse component, affected by the presence of clouds, aerosols, surface albedo, and altitude. For the investigated sites, the trend is similar for all the years with a slight alteration in 2018 due to decreased amount of clouds, which brought overall lower values of $PAR_{diffuse}$. The annual mean $PAR_{diffuse}$ value for the locations studied was 46.65 W/m^2, marginally lower (59 W/m^2) than the one reported by Lozano et al. (2022) in Granada (Spain) 2008-2018 and higher (35 W/m^2) than the one reported by Trisolino et al. (2018) in Lampedusa (Italy) 2002-2016. Since there are scarce studies about PAR trends, the comparison is made to available studies in these Southern European locations. It is interesting to observe that the $PAR_{diffuse}$ is rather similar regardless of whether it is in the north or south of Europe.

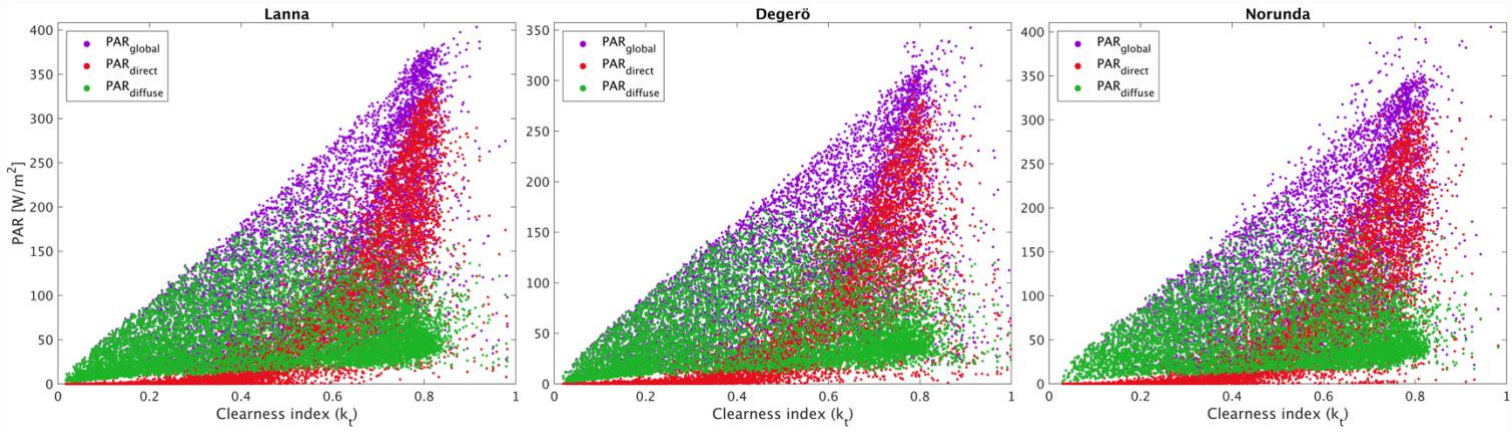

Figure 7. Scatterplots between the clearness index and PAR_{global}, PAR_{direct} and $PAR_{diffuse}$ for the period 2016 – 2018 at the studied ICOS Sweden network stations: Lanna (left), Degerö (middle), and Norunda (right). Hourly values at midpoint are used.

Figure 7 presents the effect of cloudiness on PAR_{global}, PAR_{direct} and $PAR_{diffuse}$ measurements for the investigated sites during the studied period. The upper envelope of PAR_{global} increases linearly with the clearness index. When the clearness index is low, $k_t < 0.3$, corresponding to thick cloud conditions (Chen et al., 2009), $PAR_{diffuse}$ makes the primary contribution to PAR_{global}. $PAR_{diffuse}$ increases with increasing k_t, peaking at values of k_t around 0.5 under thin cloud conditions ($0.3 \leq k_t < 0.7$), and then decreases towards clear-sky conditions, at high values of k_t. PAR_{direct} increases exponentially when the sky starts having clearer conditions ($k_t > 0.3$), and rapidly increases after the $PAR_{diffuse}$ decreases ($k_t > 0.7$). At high values of k_t, PAR_{direct} significantly contributes to the PAR_{global}. These trends are consistent across the three studied sites and align with Li et al.'s (2020) findings in a desert environment in the northern hemisphere. However, the magnitude of the PAR_{global} in this study are halved due to the climate and latitude characteristics.

The analysis demonstrates that the seasonality variation of PAR components and the relationship with cloudiness in high latitudes is similar to mid-latitudes in the northern hemisphere. However, the magnitude of the PAR components decreases as the location moves further north. This decrease is particularly noticeable for the PAR_{direct} component due to the distinct course of the solar zenith angle throughout the year resulting in reduced solar radiation. The $PAR_{diffuse}$ component, on the other hand, appears to have minor variability across seasons and locations, indicating that it is less influenced by incoming solar irradiance and more likely to be affected by sky conditions and atmospheric aerosols content.

4.3 Cases: application of CLY separation model under different data availability

To showcase the versatility of the CLY PAR separation model and its application in different scenarios, three additional use cases are demonstrated on an actual agrivoltaic site in Sweden.

4.3.1 Case 1

The results of the first case, where the CLY PAR separation model is applied exclusively with inputs gathered from satellite-derived databases or derived from algorithms, are depicted in Figure 8 – left. The model coefficients are calibrated using the combined data from the three ICOS network stations (Lanna, Degerö, and Norunda), which were previously used to evaluate the model's performance (Table 5). The aim is to illustrate the possibility of calibrating the model with available data from nearby stations that could represent the climate of the location under study. As expected, the accuracy is lower than the one obtained during the model validation, mainly due to the low spatial resolution of the CERES satellite-derived observations.

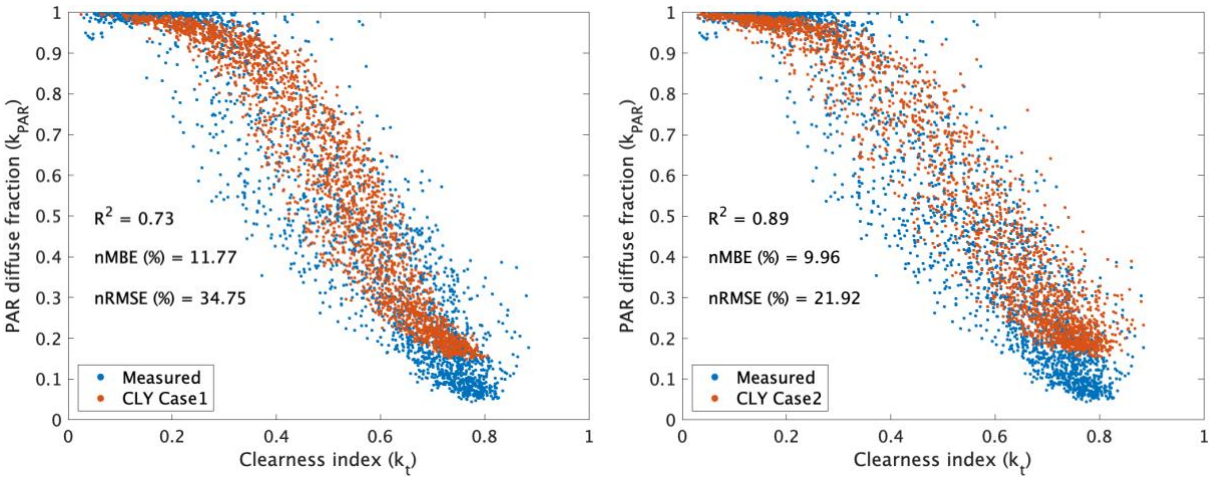

Figure 8. PAR diffuse fraction measured data plotted against the clearness index for the agrivoltaic site near Västerås. The estimated results from the proposed PAR separation model CLY are overlaid. The total number of data points (2374) in each plot refers to the dataset described in Section 2.3 and satellite-derived data after quality control. The nRMSE [%], nMBE [%] and R^2 are displayed. Left: results of Case 1. Right: results of Case 2.

The agrivoltaic site being studied covers a relatively small area and is surrounded by forest and various types of vegetation within a radius of less than 1 km (Figure 9). When the pixel size of the satellite-derived product is greater than for instance 1 km², the input parameters are usually averaged to that pixel size (Yagli et al., 2020), resulting in the inclusion of different environmental conditions that may not be fully representative of the specific agrivoltaic site conditions. Nevertheless, the results still indicate an acceptable first approximation, with an nRMSE of 34.75% and an R^2 of 0.73 for such a small experimental agrivoltaic site. It is worth noting that the accuracy could be further improved for larger agrivoltaic systems, as they would cover a much larger area and potentially benefit from better spatial representation in the satellite-derived data.

Table 5. Model coefficients of the proposed CLY PAR separation model fitted via non-linear regression least-squares method to: the combined 3 ICOS stations in Sweden with hourly time step (Lanna, Degerö, and Norunda) with 2 years of data corresponding to the period 2016-2017, and, to the agrivoltaic site near Västerås with 2/3 of the data described in Section 2.3.

	C	β_0	β_1	β_2	β_3	β_4	β_5	β_6	β_7	β_8	β_9	β_{10}
ICOS combined	0.0946	-1.1230	5.6100	-0.0820	0.0084	-1.7992	-0.5080	-0.1209	-0.8215	0.0426	0.5262	-1.4605
Agrivoltaic site	0.0439	0.3510	6.2064	-0.0152	-0.0276	5.7983	-0.2302	-2.9454	1.6568	0.0254	0.4526	-1.2059

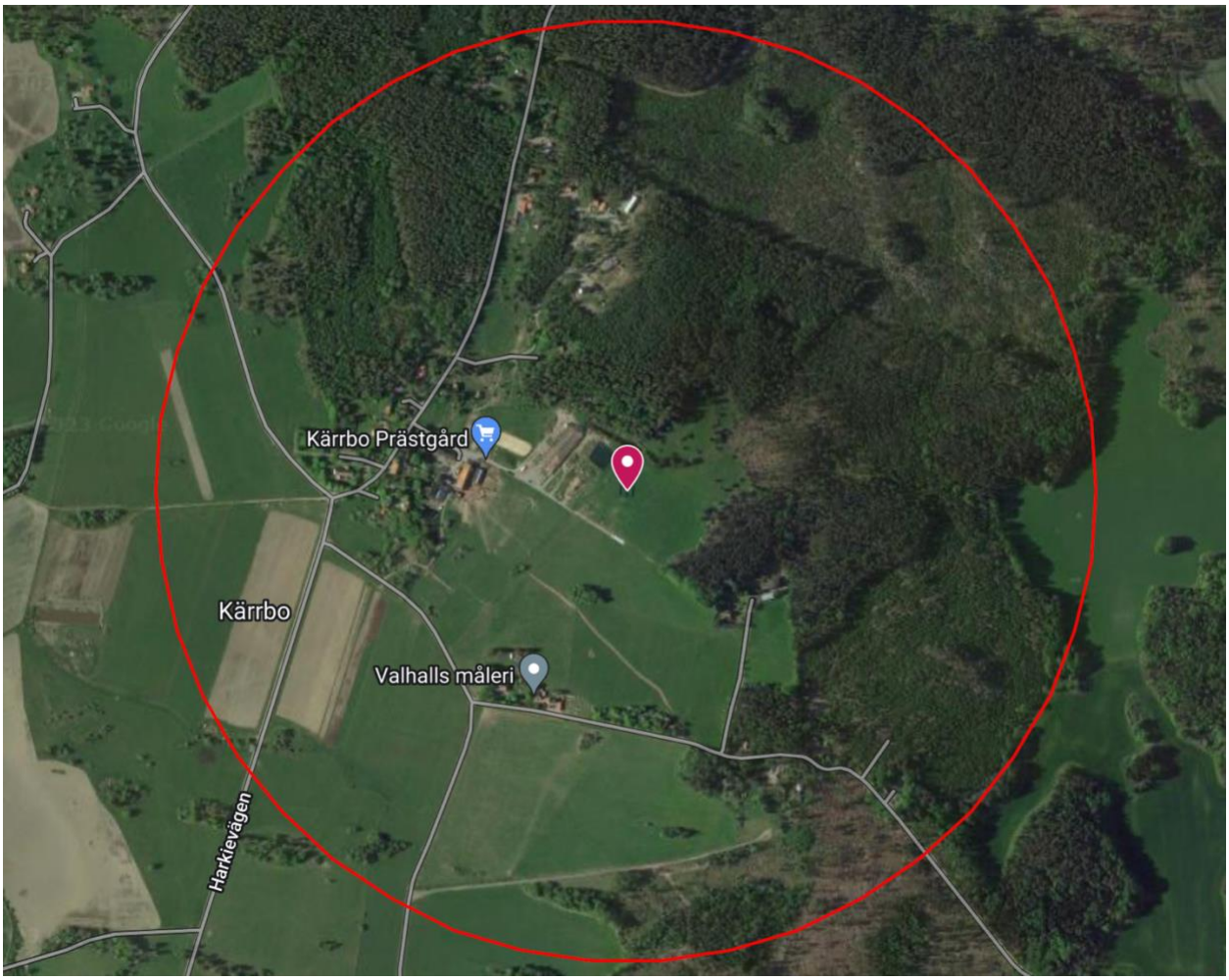

Figure 9. Satellite image of the agrivoltaic site (red marker) near Västerås, Sweden. Red circle of radius 750 m with the agrivoltaic system in the centre, illustrating the variety of terrain surrounding the site *(Google Maps, 2023)*.

4.3.2 Case 2

Like Case 1, the CLY model used in this scenario has coefficients calibrated based on the combined data from the three ICOS network stations (Table 5). However, in this case, the calibrated CLY model is provided with input data directly measured from the specific agrivoltaic site under study. The analysis period is the same as in Case 1, and the results are presented in Figure 8 – right. Compared to Case 1, this second approach demonstrates higher accuracy, with an nRMSE of 21.92%. The second case allows for a

more precise estimation of the PAR diffuse fraction, and consequently the PAR diffuse itself, as the global solar radiation components, air temperature, and relative humidity are all measured in-situ. This higher accuracy is due to the availability of specific and reliable data obtained directly from the agrivoltaic site, ensuring a faithful representation of the site's conditions.

4.3.3 Case 3

Ideally, a full year of in-situ measurements, representing all seasons, would be available for calibrating the model. However, due to data limitations, a shorter period was used in this study (April – December 2022). The results of the CLY model, fitted to the agrivoltaic site (Table 5) and evaluated with testing data, show satisfactory performance (Figure 10 – left), similar to the model evaluation results.

To further compare this approach with Case 2, the same testing data is used, and the results are displayed in Figure 10 – middle. It is evident that the model with locally fitted coefficients performs better than the model calibrated to the ICOS network stations. Additionally, the ERBS model is also evaluated with the same testing data, and the results are presented in Figure 10 – right. The single-parameter model cannot adequately represent the data spread. This results in both underestimation and overestimation of the diffuse fraction of PAR as observed, leading to inaccurate predictions of the radiation reaching the crops in an agrivoltaic system. The nMBE clearly indicates that applying ERBS model, the predictions are generally overestimated by 10%, a much larger error compared to the CLY model.

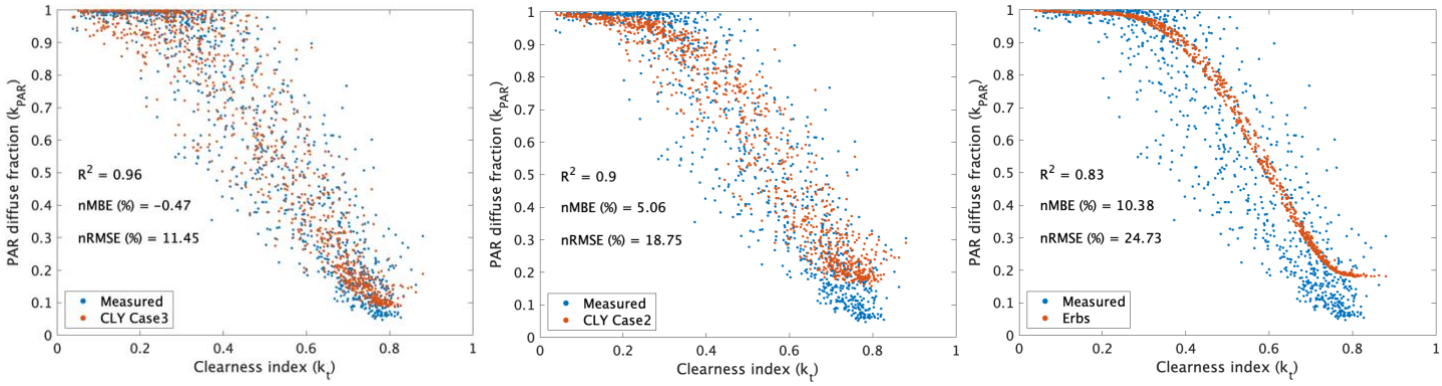

Figure 10. PAR diffuse fraction measured data plotted against the clearness index for the agrivoltaic site close to Västerås. The estimated results from the proposed PAR separation model CLY are overlaid. The total number of data points (994) in each plot refers to 1/3 of the dataset described in Section 2.3, where 2/3 of the dataset (1930 data points) are used for model calibration. The nRMSE [%], nMBE [%] and R^2 are displayed. Left: results of applying CLY model with locally calibrated coefficients – Case 3. Middle: results of applying CLY model with coefficients calibrated to the combined data of 3 ICOS-Sweden stations – Case 2. Right: results of applying ERBS model.

Different approaches for applying the CLY PAR separation model, depending on data availability, have been demonstrated for an agrivoltaic system in a high-latitude region. The following recommendations can be made: if no measured data is available, the CLY model can be calibrated to nearby stations where data is available. Then, satellite-derived data can be used as a preliminary replacement, particularly if the studied site corresponds to a large area with relatively homogenous topography and vegetation. While the ERBS single-parameter model may provide a satisfactory overall accuracy (nRMSE < 25% and R^2 > 0.8) due to

balancing positive and negative errors over time, it cannot capture the variability of the PAR diffuse fraction for the same value of k_t. To achieve higher accuracy of the diffuse PAR fraction (nRMSE < 19% and $R^2 \geq$ 0.9), the CLY PAR separation model can be applied with coefficients calibrated to nearby stations with the required predictors measured in-situ. The highest accuracy is obtained when the model's output is locally known for a specific period, ideally at least one year to cover all seasons. This approach allows the model to be accurately calibrated for the specific location, and then fed with in-situ measurements for its predictors.

5. Conclusions

The issue of conflicting land use between agricultural activities and ground-mounted solar photovoltaic power plants has become increasingly prevalent in recent years, and agrivoltaic systems offer a potential solution to this problem. Accurately estimating $PAR_{diffuse}$ is crucial for analysing agrivoltaic systems, as crops situated underneath do not receive PAR_{global} in a uniform manner, as is the case in open-field conditions. Instead, they receive a non-uniform combination of $PAR_{diffuse}$ and PAR_{direct} due to the shading produced by the PV system, with shaded areas receiving a greater proportion of $PAR_{diffuse}$. This shading typically reduces crop yields, making accurate calculation of $PAR_{diffuse}$ essential for more precise crop yield predictions.

To this end, the present study proposes a new separation model called CLY, which calculates $PAR_{diffuse}$ using the YANG2 decomposition model for GHI (Yang and Boland, 2019) as a basis. The CLY model adds four additional predictors found relevant in previous studies, namely ground albedo, optical thickness, vapour pressure deposition and aerosol optical depth.

The accuracy of the model has been compared to that of two previously identified best GHI separation models for PAR (Ma Lu et al., 2022), namely YANG2 and STARKE, and two purposedly developed PAR separation models, namely KATHILANKAL and LOZANO, across different locations in Sweden. Results show that the CLY model outperforms all the compared models in all the studied locations. Across all locations, the model achieves R^2 values above 0.90, with an improvement between 1-17% in terms of R^2 when compared to the other studied models. Although the CLY model has only been validated in three locations at high northern latitude (>58°N), primarily chosen because of the lack of studies in these regions, it could be subject to further studies to investigate its applicability and performance in other climates and at other temporal resolutions.

The developed PAR separation model was further applied to a site near Västerås, Sweden, where the country's first agrivoltaic system is being investigated. Several cases were examined, considering different

data availability scenarios. In cases where no in-situ measurements are available, the results indicate that the CLY model can be calibrated using data from nearby stations. Subsequently, satellite-derived data can serve as a substitute, particularly if the site under study is vast and has uniform topography and vegetation. Even though ERBS single-parameter model, commonly used in PV simulation software to decompose GHI, cannot fully illustrate the variability of PAR diffuse fraction for the same value of k_t, its predictions tend to balance positive and negative errors over time, resulting in a satisfactory level of accuracy. To improve the estimation of the diffuse PAR fraction, the CLY PAR separation model can be employed with coefficients calibrated to nearby stations, provided the necessary predictors are measured in-situ. Naturally, the greatest accuracy is achieved when the model's output is known for a specific period, preferable at least one year to account for all seasons. This allows for precise calibration of the model at a particular location, as the model's predictors are based on measurements gathered on-site. All the presented scenarios in this work were validated using in-situ $PAR_{diffuse}$ measurements obtained above the canopy in an open-field reference environment (downwelling PAR radiation). Moving forward, the CLY PAR separation model will be integrated into the research group's agrivoltaic integrated crop yield and PV power production model. The predictions of $PAR_{diffuse}$ will be spatially validated at the canopy level in the agrivoltaic system, accounting for the shading effects induced by the PV panels.

Acknowledgements

The authors would like to acknowledge the financial support received from the Swedish Energy Agency through the SOLVE project (grant number 52693-1). Author Pietro Elia Campana would like to acknowledge Formas - the Swedish Research Council for Sustainable Development - for the funding received through the early career project "Avoiding conflicts between the sustainable development goals through agro-photovoltaic systems" (grant number FR-2021/0005). The authors also acknowledge the Swedish Energy Agency for their financial support through the projects "Evaluation of the first agrivoltaic system in Sweden" (grant number 51000-1) and “Evaluation of the first agrivoltaic system facility in Sweden to compare commercially available agrivoltaic technologies - MATRIX” (grant number P2022-00809).

The authors would also like to acknowledge ICOS Sweden for providing the data from the Lanna, Degerö, and Norunda stations. ICOS Sweden is funded by the Swedish Research Council as a national research infrastructure. Lastly, the authors would like to thank Dejwakh Kathleen for her assistance in better understanding the satellite-derived data obtained from the NASA Langley Research Center CERES ordering tool at https://ceres.larc.nasa.gov/data/.

Conflict of Interest Statement

The authors have no conflicts to disclose.

CRediT author statement

Silvia Ma Lu: Conceptualization, Methodology, Data Curation, Formal analysis, Validation, Visualization, Writing - Original Draft, Writing - Review & Editing; **Dazhi Yang**: Writing - Review & Editing; **Martha C. Anderson**: Writing - Review & Editing; **Sebastian Zainali**: Writing - Review & Editing; **Bengt Stridh**: Writing - Review & Editing; **Anders Avelin**: Writing - Review & Editing; **Pietro Elia Campana**: Funding acquisition, Conceptualization, Methodology, Writing - Review & Editing.

Data Availability Statement

The data that support the findings of this study are available in ICOS Data Portal and upon reasonable request from the corresponding author.

References

Adeh, E.H., Good, S.P., Calaf, M., Higgins, C.W., 2019. Solar PV Power Potential is Greatest Over Croplands. Sci. Rep. 9, 11442. https://doi.org/10.1038/s41598-019-47803-3

Akitsu, T., Kume, A., Hirose, Y., Ijima, O., Nasahara, K.N., 2015. On the stability of radiometric ratios of photosynthetically active radiation to global solar radiation in Tsukuba, Japan. Agric. For. Meteorol. 209–210, 59–68. https://doi.org/10.1016/j.agrformet.2015.04.026

Alados, I., Foyo-Moreno, I., Alados-Arboledas, L., 1996. Photosynthetically active radiation: measurements and modelling. Agric. For. Meteorol. 78, 121–131. https://doi.org/10.1016/0168-1923(95)02245-7

Barenbrug, A.W.T., 1974. Psychrometry and psychrometric charts, 3d ed. ed. Chamber of Mines of South Africa, Johannesburg.

Barron-Gafford, G.A., Pavao-Zuckerman, M.A., Minor, R.L., Sutter, L.F., Barnett-Moreno, I., Blackett, D.T., Thompson, M., Dimond, K., Gerlak, A.K., Nabhan, G.P., Macknick, J.E., 2019. Agrivoltaics provide mutual benefits across the food–energy–water nexus in drylands. Nat. Sustain. 2, 848–855. https://doi.org/10.1038/s41893-019-0364-5

Bird, R.E., Riordan, C., 1986. Simple Solar Spectral Model for Direct and Diffuse Irradiance on Horizontal and Tilted Planes at the Earth's Surface for Cloudless Atmospheres. J. Clim. Appl. Meteorol. 25, 87–97. https://doi.org/10.1175/1520-0450(1986)025<0087:SSSMFD>2.0.CO;2

Brodam Galacho, C., 2023. Over 1000 visitors experienced cutting-edge agricultural research at AU Viborg [WWW Document]. URL https://agro.au.dk/en/current-news/news/show/artikel/over-1000-besoegende-oplevede-banebrydende-landbrugsforskning-hos-au-viborg (accessed 8.22.23).

Campana, P.E., Stridh, B., Amaducci, S., Colauzzi, M., 2021. Optimisation of vertically mounted agrivoltaic systems. J. Clean. Prod. 325, 129091. https://doi.org/10.1016/j.jclepro.2021.129091

Carrara, A., Kolari, P., De Beeck, M.O., Arriga, N., Berveiller, D., Dengel, S., Ibrom, A., Merbold, L., Rebmann, C., Sabbatini, S., Serrano-Ortíz, P., Biraud, S.C., 2018. Radiation measurements at ICOS ecosystem stations. Int. Agrophysics 32, 589–605. https://doi.org/10.1515/intag-2017-0049

Chen, J., Shen, M., Kato, T., 2009. Diurnal and seasonal variations in light-use efficiency in an alpine meadow ecosystem: causes and implications for remote sensing. J. Plant Ecol. 2, 173–185. https://doi.org/10.1093/jpe/rtp020

de Blas, M., García-Rodríguez, A., García, I., Torres, J.L., 2022. Validation and calibration of models to estimate photosynthetically active radiation considering different time scales and sky conditions. Adv. Space Res. 70, 1737–1760. https://doi.org/10.1016/j.asr.2022.07.005

Doelling, D., 2017. CERES Level 3 SYN1deg-1Hour Terra-Aqua-MODIS HDF4 file - Edition 4A. https://doi.org/10.5067/TERRA+AQUA/CERES/SYN1DEG-1HOUR_L3.004A

Duffie, J.A., Beckman, W.A., 2013. Solar engineering of thermal processes / John A. Duffie, William A. Beckman, 4th ed. ed. John Wiley, Hoboken.

ECMWF, 2022. CAMS-AOD [WWW Document]. SoDa. URL https://www.soda-pro.com/web-services/atmosphere/cams-aod (accessed 10.20.22).

Emde, C., Buras-Schnell, R., Kylling, A., Mayer, B., Gasteiger, J., Hamann, U., Kylling, J., Richter, B., Pause, C., Dowling, T., Bugliaro, L., 2016. The libRadtran software package for radiative transfer calculations (version 2.0.1). Geosci. Model Dev. 9, 1647–1672. https://doi.org/10.5194/gmd-9-1647-2016

F. Holmgren, W., W. Hansen, C., A. Mikofski, M., 2018. pvlib python: a python package for modeling solar energy systems. J. Open Source Softw. 3, 884. https://doi.org/10.21105/joss.00884

Ferrera-Cobos, F., Vindel, J.M., Valenzuela, R.X., González, J.A., 2020. Analysis of Spatial and Temporal Variability of the PAR/GHI Ratio and PAR Modeling Based on Two Satellite Estimates. Remote Sens. 12, 1262. https://doi.org/10.3390/rs12081262

GADM, 2022. GADM [WWW Document]. GADM. URL https://www.gadm.org (accessed 5.2.20).

García-Rodríguez, A., García-Rodríguez, S., Díez-Mediavilla, M., Alonso-Tristán, C., 2020. Photosynthetic Active Radiation, Solar Irradiance and the CIE Standard Sky Classification. Appl. Sci. 10, 8007. https://doi.org/10.3390/app10228007

Gneiting, T., 2011. Making and Evaluating Point Forecasts. J. Am. Stat. Assoc. 106, 746–762. https://doi.org/10.1198/jasa.2011.r10138

González, J.A., Calbó, J., 2002. Modelled and measured ratio of PAR to global radiation under cloudless skies. Agric. For. Meteorol. 110, 319–325. https://doi.org/10.1016/S0168-1923(01)00291-X

Google Maps, 2023. Kärrbo Prästgård [WWW Document]. URL https://maps.google.com (accessed 8.23.23).

Gu, L., Baldocchi, D., Verma, S.B., Black, T.A., Vesala, T., Falge, E.M., Dowty, P.R., 2002. Advantages of diffuse radiation for terrestrial ecosystem productivity: ADVANTAGES OF DIFFUSE RADIATION. J. Geophys. Res. Atmospheres 107, ACL 2-1-ACL 2-23. https://doi.org/10.1029/2001JD001242

Gu, L., Fuentes, J.D., Shugart, H.H., Staebler, R.M., Black, T.A., 1999. Responses of net ecosystem exchanges of carbon dioxide to changes in cloudiness: Results from two North American deciduous forests. J. Geophys. Res. Atmospheres 104, 31421–31434. https://doi.org/10.1029/1999JD901068

Gueymard, C., 1995. Simple Model for the Atmospheric Radiative Transfer of Sunshine (SMARTS2) Algorithms and performance assessment 84.

Gueymard, C.A., 2018. Revised composite extraterrestrial spectrum based on recent solar irradiance observations. Sol. Energy 169, 434–440. https://doi.org/10.1016/j.solener.2018.04.067

Hao, D., Asrar, G.R., Zeng, Y., Zhu, Q., Wen, J., Xiao, Q., Chen, M., 2019. Estimating hourly land surface downward shortwave and photosynthetically active radiation from DSCOVR/EPIC observations. Remote Sens. Environ. 232, 111320. https://doi.org/10.1016/j.rse.2019.111320

Hersbach, H., Bell, B., Berrisford, P., Biavati, G., Horány, A., Muñoz Sabater, J., Nicolas, J., Peubey, C., Radu, R., Rozum, I., Schepers, D., Simmons, A., Soci, C., Dee, D., Thépaut, J.-N., 2023. ERA5 hourly data on single levels from 1940 to present. https://doi.org/10.24381/cds.adbb2d47

Hu, B., Wang, Y., Liu, G., 2007. Spatiotemporal characteristics of photosynthetically active radiation in China. J. Geophys. Res. 112, D14106. https://doi.org/10.1029/2006JD007965

ICOS Sweden [WWW Document], 2022. URL https://www.icos-sweden.se/ (accessed 10.6.22).

Ineichen, P., 2008. A broadband simplified version of the Solis clear sky model. Sol. Energy 82, 758–762. https://doi.org/10.1016/j.solener.2008.02.009

Jacovides, C.P., Boland, J., Asimakopoulos, D.N., Kaltsounides, N.A., 2010. Comparing diffuse radiation models with one predictor for partitioning incident PAR radiation into its diffuse component in the eastern Mediterranean basin. Renew. Energy 35, 1820–1827. https://doi.org/10.1016/j.renene.2009.11.015

Jacovides, C.P., Tymvios, F.S., Asimakopoulos, D.N., Theofilou, K.M., Pashiardes, S., 2003. Global photosynthetically active radiation and its relationship with global solar radiation in the Eastern Mediterranean basin. Theor. Appl. Climatol. 74, 227–233. https://doi.org/10.1007/s00704-002-0685-5

Janjai, S., Wattan, R., 2011. Development of a model for the estimation of photosynthetically active radiation from geostationary satellite data in a tropical environment. Remote Sens. Environ. 115, 1680–1693. https://doi.org/10.1016/j.rse.2011.02.026

Kanniah, K.D., Beringer, J., North, P., Hutley, L., 2012. Control of atmospheric particles on diffuse radiation and terrestrial plant productivity: A review. Prog. Phys. Geogr. Earth Environ. 36, 209–237. https://doi.org/10.1177/0309133311434244

Kasten, F., Young, A.T., 1989. Revised optical air mass tables and approximation formula. Appl. Opt. 28, 4735. https://doi.org/10.1364/AO.28.004735

Kathilankal, J.C., O'Halloran, T.L., Schmidt, A., Hanson, C.V., Law, B.E., 2014. Development of a semi-parametric PAR (Photosynthetically Active Radiation) partitioning model for the United States, version 1.0. Geosci. Model Dev. 7, 2477–2484. https://doi.org/10.5194/gmd-7-2477-2014

Keane, B.J., Ineson, P., Vallack, H.W., Blei, E., Bentley, M., Howarth, S., McNamara, N.P., Rowe, R.L., Williams, M., Toet, S., 2018. Greenhouse gas emissions from the energy crop oilseed rape (*Brassica napus*); the role of photosynthetically active radiation in diurnal N_2O flux variation. GCB Bioenergy 10, 306–319. https://doi.org/10.1111/gcbb.12491

Koblick, D., 2021. Vectorized Solar Azimuth and Elevation Estimation [WWW Document]. MATLAB Cent. File Exch. URL https://se.mathworks.com/matlabcentral/fileexchange/23051-vectorized-solar-azimuth-and-elevation-estimation (accessed 12.9.21).

Li, C., Jia, X., Ma, J., Liu, P., Yang, R., Bai, Y., Hayat, M., Liu, J., Zha, T., 2020. Linking diffuse radiation and ecosystem productivity of a desert steppe ecosystem. PeerJ 8, e9043. https://doi.org/10.7717/peerj.9043

Li, R., Zhao, L., Ding, Y., Wang, S., Ji, G., Xiao, Y., Liu, G., Sun, L., 2010. Monthly ratios of PAR to global solar radiation measured at northern Tibetan Plateau, China. Sol. Energy 84, 964–973. https://doi.org/10.1016/j.solener.2010.03.005

López, G., Rubio, M.A., Martínez, M., Batlles, F.J., 2001. Estimation of hourly global photosynthetically active radiation using artificial neural network models. Agric. For. Meteorol. 107, 279–291. https://doi.org/10.1016/S0168-1923(01)00217-9

Lozano, I.L., Sánchez-Hernández, G., Guerrero-Rascado, J.L., Alados, I., Foyo-Moreno, I., 2022. Analysis of cloud effects on long-term global and diffuse photosynthetically active radiation at a Mediterranean site. Atmospheric Res. 268, 106010. https://doi.org/10.1016/j.atmosres.2021.106010

Lu, H., Qin, Z., Lin, S., Chen, X., Chen, B., He, B., Wei, J., Yuan, W., 2022. Large influence of atmospheric vapor pressure deficit on ecosystem production efficiency. Nat. Commun. 13, 1653. https://doi.org/10.1038/s41467-022-29009-w

Ma Lu, S., Zainali, S., Stridh, B., Avelin, A., Amaducci, S., Colauzzi, M., Campana, P.E., 2022. Photosynthetically active radiation decomposition models for agrivoltaic systems applications. Sol. Energy 244, 536–549. https://doi.org/10.1016/j.solener.2022.05.046

Mamun, M.A.A., Dargusch, P., Wadley, D., Zulkarnain, N.A., Aziz, A.A., 2022. A review of research on agrivoltaic systems. Renew. Sustain. Energy Rev. 161, 112351. https://doi.org/10.1016/j.rser.2022.112351

Mariscal, MariaJ., Martens, ScottN., Ustin, SusanL., Chen, J., Weiss, StuartB., Roberts, DarA., 2004. Light-transmission Profiles in an Old-growth Forest Canopy:Simulations of Photosynthetically

Active Radiation by Using Spatially Explicit Radiative Transfer Models. Ecosystems 7. https://doi.org/10.1007/s10021-004-0137-4
MathWorks, 2023. fitnlm [WWW Document]. URL https://se.mathworks.com/help/stats/fitnlm.html (accessed 6.1.23).
McCree, K.J., 1972. Test of current definitions of photosynthetically active radiation against leaf photosynthesis data. Agric. Meteorol. 10, 443–453. https://doi.org/10.1016/0002-1571(72)90045-3
McCree, K.J., 1971. The action spectrum, absorptance and quantum yield of photosynthesis in crop plants. Agric. Meteorol. 9, 191–216. https://doi.org/10.1016/0002-1571(71)90022-7
Mercado, L.M., Bellouin, N., Sitch, S., Boucher, O., Huntingford, C., Wild, M., Cox, P.M., 2009. Impact of changes in diffuse radiation on the global land carbon sink. Nature 458, 1014–1017. https://doi.org/10.1038/nature07949
Mizoguchi, Y., Ohtani, Y., Aoshima, T., Hirakata, A., Yuta, S., Takanashi, S., Iwata, H., Nakai, Y., 2010. Comparison of the characteristics of five quantum sensors. Bull. FFPRI 9, 113–120.
Niu, Z., Wang, L., Niu, Y., Hu, B., Zhang, M., Qin, W., 2019. Spatiotemporal variations of photosynthetically active radiation and the influencing factors in China from 1961 to 2016. Theor. Appl. Climatol. 137, 2049–2067. https://doi.org/10.1007/s00704-018-2727-7
Noriega Gardea, M.M.A., Corral Martínez, L.F., Anguiano Morales, M., Trujillo Schiaffino, G., Salas Peimbert, D.P., 2020. MODELLING PHOTOSYNTHETICALLY ACTIVE RADIATION: A REVIEW. Atmósfera. https://doi.org/10.20937/ATM.52737
Nwokolo, S., 2018. A Global Review of Empirical Models for Estimating Photosynthetically Active Radiation. Trends Renew. Energy 4. https://doi.org/10.17737/tre.2018.4.2.0079
Oliphant, A.J., Stoy, P.C., 2018. An Evaluation of Semiempirical Models for Partitioning Photosynthetically Active Radiation Into Diffuse and Direct Beam Components. J. Geophys. Res. Biogeosciences 123, 889–901. https://doi.org/10.1002/2017JG004370
Oliveira, A.P., Escobedo, J.F., Machado, A.J., Soares, J., 2002. Correlation models of diffuse solar-radiation applied to the city of São Paulo, Brazil. Appl. Energy 71, 59–73. https://doi.org/10.1016/S0306-2619(01)00040-X
Olseth, J., 1997. Spatial distribution of photosynthetically active radiation over complex topography. Agric. For. Meteorol. 86, 205–214. https://doi.org/10.1016/S0168-1923(97)00010-5
Orgill, J.F., Hollands, K.G.T., 1977. Correlation equation for hourly diffuse radiation on a horizontal surface. Sol. Energy 19, 357–359. https://doi.org/10.1016/0038-092X(77)90006-8
Proutsos, N.D., Liakatas, A., Alexandris, S.G., Tsiros, I.X., Tigkas, D., Halivopoulos, G., 2022. Atmospheric Factors Affecting Global Solar and Photosynthetically Active Radiation Relationship in a Mediterranean Forest Site. Atmosphere 13, 1207. https://doi.org/10.3390/atmos13081207
Räisänen, J., 2019. Energetics of interannual temperature variability. Clim. Dyn. 52, 3139–3156. https://doi.org/10.1007/s00382-018-4306-0
Ren, X., He, H., Zhang, L., Yu, G., 2018. Global radiation, photosynthetically active radiation, and the diffuse component dataset of China, 1981–2010. Earth Syst. Sci. Data 10, 1217–1226. https://doi.org/10.5194/essd-10-1217-2018
Ridley, B., Boland, J., Lauret, P., 2010. Modelling of diffuse solar fraction with multiple predictors. Renew. Energy 35, 478–483. https://doi.org/10.1016/j.renene.2009.07.018
Schaaf, C., Wang, Z., 2021. MODIS/Terra+Aqua BRDF/Albedo Model Parameters Daily L3 Global - 500m V061. https://doi.org/10.5067/MODIS/MCD43A1.061
Sinclair, V.A., Mikkola, J., Rantanen, M., Räisänen, J., 2019. The summer 2018 heatwave in Finland. Weather 74, 403–409. https://doi.org/10.1002/wea.3525
Skartveit, A., Olseth, J.A., 1987. A model for the diffuse fraction of hourly global radiation. Sol. Energy 38, 271–274. https://doi.org/10.1016/0038-092X(87)90049-1

Soares, J., Oliveira, A.P., Božnar, M.Z., Mlakar, P., Escobedo, J.F., Machado, A.J., 2004. Modeling hourly diffuse solar-radiation in the city of São Paulo using a neural-network technique. Appl. Energy 79, 201–214. https://doi.org/10.1016/j.apenergy.2003.11.004

Sojib Ahmed, M., Rezwan Khan, M., Haque, A., Ryyan Khan, M., 2022. Agrivoltaics analysis in a techno-economic framework: Understanding why agrivoltaics on rice will always be profitable. Appl. Energy 323, 119560. https://doi.org/10.1016/j.apenergy.2022.119560

Spencer, J. W, 1971. Fourier Series Representation of the Position of the Sun. Search 2, 172.

Spitters, C.J.T., Toussaint, H.A.J.M., Goudriaan, J., 1986. Separating the diffuse and direct component of global radiation and its implications for modeling canopy photosynthesis Part I. Components of incoming radiation. Agric. For. Meteorol. 38, 217–229. https://doi.org/10.1016/0168-1923(86)90060-2

Starke, A.R., Lemos, L.F.L., Boland, J., Cardemil, J.M., Colle, S., 2018. Resolution of the cloud enhancement problem for one-minute diffuse radiation prediction. Renew. Energy 125, 472–484. https://doi.org/10.1016/j.renene.2018.02.107

Su, W., Charlock, T.P., Rose, F.G., Rutan, D., 2007. Photosynthetically active radiation from Clouds and the Earth's Radiant Energy System (CERES) products. J. Geophys. Res. 112, G02022. https://doi.org/10.1029/2006JG000290

Tan, C., Wang, D., Zhou, J., Du, Y., Luo, M., Zhang, Y., Guo, W., 2018. Remotely Assessing Fraction of Photosynthetically Active Radiation (FPAR) for Wheat Canopies Based on Hyperspectral Vegetation Indexes. Front. Plant Sci. 9, 776. https://doi.org/10.3389/fpls.2018.00776

Technical Committee on Standardization of Reference Evapotranspiration, 2005. The ASCE Standardized Reference Evapotranspiration Equation. American Society of Civil Engineers, Reston, VA. https://doi.org/10.1061/9780784408056

Thomas, C., Dorling, S., Wandji Nyamsi, W., Wald, L., Rubino, S., Saboret, L., Trolliet, M., Wey, E., 2019. Assessment of five different methods for the estimation of surface photosynthetically active radiation from satellite imagery at three sites – application to the monitoring of indoor soft fruit crops in southern UK. Adv. Sci. Res. 16, 229–240. https://doi.org/10.5194/asr-16-229-2019

Trisolino, P., di Sarra, A., Anello, F., Bommarito, C., Di Iorio, T., Meloni, D., Monteleone, F., Pace, G., Piacentino, S., Sferlazzo, D., 2018. A long-term time series of global and diffuse photosynthetically active radiation in the Mediterranean: interannual variability and cloud effects. Atmospheric Chem. Phys. 18, 7985–8000. https://doi.org/10.5194/acp-18-7985-2018

Trisolino, P., Sarra, A. di, Meloni, D., Pace, G., 2016. Determination of global and diffuse photosynthetically active radiation from a multifilter shadowband radiometer. Appl. Opt. 55, 8280. https://doi.org/10.1364/AO.55.008280

US Department of Commerce, N., 2021. ESRL Global Monitoring Laboratory - Global Radiation and Aerosols [WWW Document]. URL https://gml.noaa.gov/grad/solcalc/calcdetails.html (accessed 12.14.21).

Valle, B., Simonneau, T., Sourd, F., Pechier, P., Hamard, P., Frisson, T., Ryckewaert, M., Christophe, A., 2017. Increasing the total productivity of a land by combining mobile photovoltaic panels and food crops. Appl. Energy 206, 1495–1507. https://doi.org/10.1016/j.apenergy.2017.09.113

Wandji Nyamsi, W., Blanc, P., Augustine, J.A., Arola, A., Wald, L., 2019. A New Clear-Sky Method for Assessing Photosynthetically Active Radiation at the Surface Level. Atmosphere 10, 219. https://doi.org/10.3390/atmos10040219

Wang, L., Kisi, O., Zounemat-Kermani, M., Hu, B., Gong, W., 2016. Modeling and comparison of hourly photosynthetically active radiation in different ecosystems. Renew. Sustain. Energy Rev. 56, 436–453. https://doi.org/10.1016/j.rser.2015.11.068

Wang, Q., Tenhunen, J., Schmidt, M., Kolcun, O., Droesler, M., Reichstein, M., 2006. Estimation of total, direct and diffuse PAR under clear skies in complex alpine terrain of the National Park Berchtesgaden, Germany. Ecol. Model. 196, 149–162. https://doi.org/10.1016/j.ecolmodel.2006.02.005

Weiss, A., Norman, J.M., 1985. Partitioning solar radiation into direct and diffuse, visible and near-infrared components. Agric. For. Meteorol. 34, 205–213. https://doi.org/10.1016/0168-1923(85)90020-6

Wielicki, B.A., Barkstrom, B.R., Harrison, E.F., Lee, R.B., Louis Smith, G., Cooper, J.E., 1996. Clouds and the Earth's Radiant Energy System (CERES): An Earth Observing System Experiment. Bull. Am. Meteorol. Soc. 77, 853–868. https://doi.org/10.1175/1520-0477(1996)077<0853:CATERE>2.0.CO;2

Wilcke, R.A.I., Kjellström, E., Lin, C., Matei, D., Moberg, A., Tyrlis, E., 2020. The extremely warm summer of 2018 in Sweden – set in a historical context. Earth Syst. Dyn. 11, 1107–1121. https://doi.org/10.5194/esd-11-1107-2020

Williams, H.J., Hashad, K., Wang, H., Max Zhang, K., 2023. The potential for agrivoltaics to enhance solar farm cooling. Appl. Energy 332, 120478. https://doi.org/10.1016/j.apenergy.2022.120478

Willockx, B., Herteleer, B., Cappelle, J., 2020. Combining photovoltaic modules and food crops: first agrivoltaic prototype in Belgium. Renew. Energy Power Qual. J. 18, 266–271. https://doi.org/10.24084/repqj18.291

Wong, L.T., Chow, W.K., 2001. Solar radiation model. Appl. Energy 69, 191–224. https://doi.org/10.1016/S0306-2619(01)00012-5

Yagli, G.M., Yang, D., Gandhi, O., Srinivasan, D., 2020. Can we justify producing univariate machine-learning forecasts with satellite-derived solar irradiance? Appl. Energy 259, 114122. https://doi.org/10.1016/j.apenergy.2019.114122

Yang, D., Alessandrini, S., Antonanzas, J., Antonanzas-Torres, F., Badescu, V., Beyer, H.G., Blaga, R., Boland, J., Bright, J.M., Coimbra, C.F.M., David, M., Frimane, Â., Gueymard, C.A., Hong, T., Kay, M.J., Killinger, S., Kleissl, J., Lauret, P., Lorenz, E., van der Meer, D., Paulescu, M., Perez, R., Perpiñán-Lamigueiro, O., Peters, I.M., Reikard, G., Renné, D., Saint-Drenan, Y.-M., Shuai, Y., Urraca, R., Verbois, H., Vignola, F., Voyant, C., Zhang, J., 2020. Verification of deterministic solar forecasts. Sol. Energy 210, 20–37. https://doi.org/10.1016/j.solener.2020.04.019

Yang, D., Boland, J., 2019. Satellite-augmented diffuse solar radiation separation models. J. Renew. Sustain. Energy 11, 023705. https://doi.org/10.1063/1.5087463

Yang, D., Kleissl, J., 2022. Summarizing ensemble NWP forecasts for grid operators: Consistency, elicitability, and economic value. Int. J. Forecast. S016920702200111X. https://doi.org/10.1016/j.ijforecast.2022.08.002

Yu, X., Guo, X., 2016. Hourly photosynthetically active radiation estimation in Midwestern United States from artificial neural networks and conventional regressions models. Int. J. Biometeorol. 60, 1247–1259. https://doi.org/10.1007/s00484-015-1120-9

Yu, X., Wu, Z., Jiang, W., Guo, X., 2015. Predicting daily photosynthetically active radiation from global solar radiation in the Contiguous United States. Energy Convers. Manag. 89, 71–82. https://doi.org/10.1016/j.enconman.2014.09.038